isvr Institute of Sound and Vibration Research

Decentralised Velocity Feedback Control of a Resiliently Mounted Panel using a Triangular Piezoelectric Actuator

A Bracco and P Gardonio

ISVR Technical Memorandum Nº 965

September 2006

University of Southampton

SCIENTIFIC PUBLICATIONS BY THE ISVR

Technical Reports are published to promote timely dissemination of research results by ISVR personnel. This medium permits more detailed presentation than is usually acceptable for scientific journals. Responsibility for both the content and any opinions expressed rests entirely with the author(s).

Technical Memoranda are produced to enable the early or preliminary release of information by ISVR personnel where such release is deemed to the appropriate. Information contained in these memoranda may be incomplete, or form part of a continuing programme; this should be borne in mind when using or quoting from these documents.

Contract Reports are produced to record the results of scientific work carried out for sponsors, under contract. The ISVR treats these reports as confidential to sponsors and does not make them available for general circulation. Individual sponsors may, however, authorize subsequent release of the material.

UNIVERSITY OF SOUTHAMPTON

INSTITUTE OF SOUND AND VIBRATION RESEARCH

SIGNAL PROCESSING AND CONTROL GROUP

Decentralised Velocity Feedback Control of a Resiliently Mounted Panel using a Triangular Piezoelectric Actuator

by

A Bracco and P Gardonio

ISVR Technical Memorandum 965

September 2006

Authorized for issue by
Professor R. Allen
Group Chairman

ABSTRACT

This report presents the study on the stability of the response of a direct feedback control loop using triangular piezoelectric actuators bonded on smart panels. Direct velocity feedback control systems allow a good reduction of the transmitted sound through light panels. However, their performance is limited by their stability at high frequencies. Several theoretical works have shown that the triangularly shaped actuators are more efficient than the squared ones and the effect of the dimension of the actuator on the stability has already been discussed, however the influence of boundary conditions has not been studied yet. In this work, the panel is considered resiliently supported by springs in rotation and translation so that we can modify their stiffness in order to simulate several boundary conditions from free to clamped or simply supported. The boundary conditions have a big influence on the response of the panel and therefore on the stability of the system. This study shows the effect of the boundary conditions on the stability and estimate the gain applicable to the system in order to have the best control without destabilising the system.

TABLE OF CONTENTS

TABLE OF FIGURES

1. INTRODUCTION

Acoustics in automobiles have been improved in the last few years as a consequence of the legislation and the demand of comfort by customers [1]. However, in contrast to the engine vibrations which are well screened today, tyre noise and aerodynamic noise such as turbulence created by the rear-view mirrors still come through the cockpit and create disturbances for the passengers. A major problem of acoustic passive insulation systems is their price as well as their size and weight which are not compatible with the constructors' policy of decreasing cost and lightening vehicles.

There are two ways of reducing the level of sound in the cockpit, the first approach aims to decrease the source of noise while the second aims to reduce the transmission of this noise [2]. This study is focused on the reduction of the transmission of noise through a light panel with active control system [2]. In contrast to passive control methods which have been proved to be efficient in the high audio frequency range but tend to be less effective in the low audio frequency range, where the mechanical responses of structures are characterised by well–separated resonances, the active system methods control low frequency vibration and sound radiation. Another advantage of active systems is their size and weight which could be rather low. Frequently both passive and active systems are used together to reduce transmitted vibration and radiated sound in a large frequency range.

Active control systems can be divided into two groups: feedforward and feedback control systems. Feedforward control systems require a reference signal well correlated to the disturbance to be controlled. Thus they normally provide good control effects for tonal disturbances that can be easily characterised far in advance [3,4]. For random disturbances, feedback control schemes should be used. These systems can provide good control performance regardless the type of disturbance to be controlled provided the sensor and actuator transducers are collocated and dual so that large feedback control gains can be implemented with no stability problems [5,6]. Feedback control systems for vibro-acoustic control can be classified in three categories: a) Multiple Input Multiple Output (MIMO) systems with fully coupled arrays of error sensor and actuators, b) Decentralised MIMO feedback control schemes with arrays of independent sensor–actuator pairs, and c) Single Input Single Output (SISO) active feedback control schemes, using distributed sensor–actuator pairs.

Fully coupled MIMO feedback systems are difficult to implement in practice, since a reliable model of the response functions between all sensors and actuators is required by the controller [5, 6]. MIMO decentralised control systems have been shown to give good control performance which are comparable to those that would be obtained from an ideal fully coupled MIMO feedback control system [7,8]. The implementation of decentralised MIMO system is much simpler than that of fully coupled systems, since simple SISO feedback loops need to be implemented. Elliott at al. [9] have shown that, provided the sensor–actuator pairs are dual and collocated [10, 11], the decentralised MIMO system is bound to be stable if direct velocity control is implemented [12]. Therefore, the main issue of decentralised MIMO control is concerned with the design of collocated and dual sensor–actuator pairs.

When decentralised velocity feedback loops are implemented in such a way as to generate active damping, both the frequency average vibration and sound radiation of the structure are reduced [8,9], provided an optimal gain is implemented such that the damping action is maximised without pinning the structure at the control positions [13]. The optimally tuned active dampers reduce the amplitudes of the well separated

low frequency resonances of the structure and thus the frequency averaged vibration and sound radiation at low frequencies.

In principle, SISO feedback control systems using distributed sensor–actuator pairs specifically designed to minimise the most efficient radiations modes of the radiating structure [14] form the simplest and most convenient solution for active structural acoustic control. However, they normally require strain transducers, such as piezoelectric transducers, which cannot be easily used in matched pairs as sensors and actuators because feed-through effects that limit the stability of the control loop [15].

Decentralised MIMO systems, which are used on the experiments for this study, offer a good compromise between the fully coupled MIMO and the distributed transducers SISO control systems.

At first a system of sixteen squared piezoelectric actuators [16, 17] has been studied giving good performances but it was limited in gain because the sensor and the actuator pairs were not collocated so that the responses were not in phase with the command. The second system envisaged is composed of sixteen triangular actuators with velocity sensors at their tips placed on the edges of the panel. The first advantage of this system is the stability because of the shape of the actuators which permit a larger gain due to the collocation of the velocity sensor and the main damping force. The second advantage is the fact the actuators are placed along the edges and act on the boundary conditions so that they can be placed on transparent elements such as windows.

Previous works by Gardonio and Elliott [18], Emo and Gardonio [19], Aoki et al. [20] and Hong et al. [21], have investigated the stability and control effect produced by a panel solidly clamped along the edges.

In the following study, the response of a flat light smart panel which is instead resiliently supported and has sixteen decentralised direct velocity feedback control systems is analysed. Each control system consists of a triangular shaped piezoelectric actuator, whose base edge is aligned at 2mm of the border of the panel, and a velocity sensor mounted at its tip. The signal given by the velocity sensor is fed back into the actuator, which generates a damping force at its tip but also bending moments on its edges and singular forces on the two other corners, which, all together, can bring the system to be unstable. As the force at the tip of the actuator is proportional to velocity, it can be considered as a damping force. Thus the sixteen independent control units generate a damping effect that tends to reduce the response of the panel in correspondence to the well-separated low frequencies resonances.

The study presented in this report is focused on the stability of one control unit in relation to the boundary conditions. This is a key study to establish whether stable loops can be can be designed and thus whether relatively large control gains can be implemented in a smart panel with such a decentralised control units. The effect of high feedback gains is to reduce efficiently the response of the panel but also could destabilise the control system, therefore a compromise has to found in order to have the best performances while the system remains stable.

This report is divided into three parts. In the first part is presented the general behaviour of a simply supported panel controlled by singular force collocated to the error sensor. In this part of the study are also introduced the tools which enable the evaluation of the stability and the performance of the control system.

In the second part we present the study of a direct velocity feedback control loop on a resiliently mounted plate. In this section we study the stability and control performance of a feedback velocity control loop for several values of mounting stiffness’s.

In the last part the performance and stability study of a smart panel resiliently supported controlled by a decentralised velocity feedback loop using a triangular piezoelectric actuator is given. A wide range of linear and angular mounting stiffness' is considered here in order to observe the behaviour of the panel and the stability of the system with reference to the rigidity of the mounting system.

2. BACKGROUND OF DIRECT VELOCITY FEEDBACK CONTROL ON A SIMPLY SUPPORTED PLATE

In order to have a first insight of the response of the light panel with a velocity feedback control loop, a simply supported panel controlled by a single force collocated to the sensor is presented. The structure studied is a simply supported rectangular aluminium thin panel to which is applied a primary force excitation at position (x_0, y_0). The control is made by a single force collocated to the error velocity sensor at the control point who is located at position (x_1, y_1) in the central area of the panel as it is presented Figure 1. The mass effects of the sensor and the actuator are not taken in account. The gain of the feedback loop is denoted by *g*.

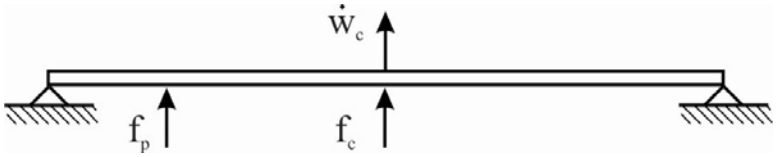

Figure 1: *Transversal schema of the panel with primary excitation force and single control force collocated to the sensor*

First the system is modelised in order to study its behaviour, that is its stability and its performance. The Euler Bernoulli theory has been used, which means only the bending waves in a thin plate structure are considered. This assumption is acceptable since the shear and rotational inertia effects become important only at very high frequencies, around 10 kHz for this panel. In the second part of this section the tools used to study the stability are presented and applied to our system as an example. The third part presents the plots used to visualise the performance at one point of the plate and the global damping effect of the system on the plate.

2.1 Modelisation

To analyse the response of the panel we need to calculate the velocity at the control point and the kinetic energy of the panel. A mobility model has therefore been build in order to derive the local and global responses of the panel as a superposition of the primary and control sources active on the panel. The mobilities of finite plates can be written in terms of a modal summation [22]. The case of a rectangular plate is considered. The main Cartesian co-ordinate system of reference (O, x, y, z) is located at the corner of the plate with the axe z axis orthogonal to the surface of the plate. The transfer functions $Y_{cp} = \frac{\dot{w}_c}{F_p}$ and $Y_{cc} = \frac{\dot{w}_c}{F_c}$ giving the velocity at the control position per unit primary and control forces are given by the following mobility functions:

$$Y_{cp} = j\omega \sum_{m=1}^{\infty} \sum_{n=1}^{\infty} \frac{\phi_{m,n}(x_c, y_c)\phi_{m,n}(x_p, y_p)}{\Lambda[\omega_{m,n}^2(1 - j\eta_s) - \omega^2]} \tag{1}$$

$$Y_{cc} = j\omega \sum_{m=1}^{\infty} \sum_{n=1}^{\infty} \frac{\phi_{m,n}(x_c, y_c)\phi_{m,n}(x_c, y_c)}{\Lambda[\omega_{m,n}^2(1 - j\eta_s) - \omega^2]} \tag{2}$$

with

$$\Lambda = \rho_s h_s l_x l_y \tag{3}$$

where $\phi_{m,n}$ is the (m,n)th natural mode of the panel and $\omega_{m,n}$ is the (m,n)th natural frequencies, η_s the damping coefficient.

The natural frequencies depend on the boundary conditions and on the characteristics of the panel. For a simply supported panel they are given by:

$$\omega_{m,n} = \sqrt{\frac{E_s I_s}{\rho_s h_s (1 - \nu_s^2)}} \left[\left(\frac{m\pi}{l_x} \right)^2 + \left(\frac{n\pi}{l_y} \right)^2 \right] = \sqrt{\frac{E_s h_s}{12\rho_s (1 - \nu_s^2)}} \left[\left(\frac{m\pi}{l_x} \right)^2 + \left(\frac{n\pi}{l_y} \right)^2 \right] \tag{4}$$

with E_s is the Young modulus, h_s the height of the panel, ν_s the Poisson coefficient, ρ_s its mass density and I_s the inertia moment. l_x and l_y are the length of the panel's edges along x and y respectively.

The natural modes also depend on the boundary conditions and are given by [22]:

$$\phi_{m,n}(x, y) = \sin\left(\frac{m\pi x}{l_x} \right) \sin\left(\frac{n\pi y}{l_y} \right) \tag{5}$$

The panel studied is an aluminium panel whose geometrical and physical characteristics are summarized in table 1.

Table 1: *Parameters of the panel*

Parameter	**Value**
Dimensions	$l_x \times l_y = 414 \times 314 mm$
Thickness	$h_p = 1 mm$
Mass density	$\rho_p = 2700 kg/m^3$
Young's modulus	$E_p = 7 \times 10^{10} N/m^2$
Poisson ratio	$\nu_p = 0.33$

2.2. Stability

This part presents the tools to study the stability of a feedback control system and an example of this type of analysis based on the feedback system controlling the simply supported panel.

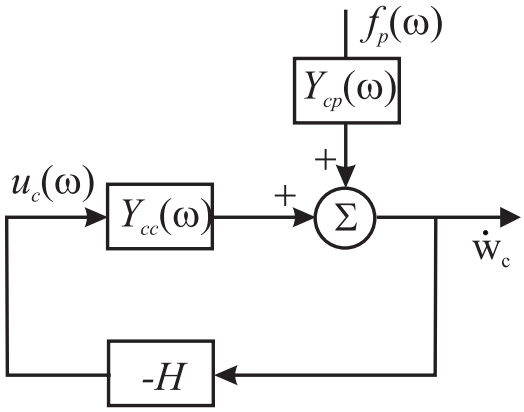

Figure 2*: Block diagram of the active control system*

The control system can be represented by a block diagram as in Figure 2. The control command $u_c(\omega)$ is given by the signal of the sensor, which measure the velocity at the error sensor, multiplied by the gain of the system. The velocity of the control point is function of the two forces, the primary excitation f_p force and the control force f_c. Therefore assuming the system is linear, the response of the system will be of the form:

$$\dot{w}_c = Y_{cc} f_c + Y_{cp} f_p \quad , \tag{6}$$

with f_p, primary excitation force and f_c, control force which as a result of direct velocity feedback loop is given by:

$$f_c = -g_c \dot{w}_c \ , \tag{7}$$

where g_c is the gain of the control system. Substituting equation (7) into equation (6), this finally gives after some mathematical manipulations the response at the control position can be expressed in terms of the primary excitation and control gain:

$$\dot{w}_c = \frac{Y_{cp}}{1 + g_c Y_{cc}} f_p \quad . \tag{8}$$

The system will become unstable if the denominator of the transfer function tends to 0 which means:

$$1 + g_c Y_{cc} = 0 \, ,$$

that is:

$$g_c Y_{cc} = -1 .$$

This indicates that the real part of the open loop transfer function has to be observed in order to study the stability of the closed loop transfer function. In fact the system will be bound to be unconditionally stable if $\mathrm{Re}\{g_c Y_{cc}\} \geq 0$. The instability, conditional stability and unconditional stability is normally assessed using the Nyquist stability criterion [23, 24].

The Nyquist stability criterion states that if the curve representing the open loop transfer function of the system in the Nyquist plot encloses the point (-1,0), the system is unstable. Also if a part of the curve belong to the left hand side of the Nyquist plot (e.g. the real part of the open loop transfer function has negative values) but the curve does not enclose the point (-1, 0), the system is conditionally stable. In this case, the system can go unstable if the gain of the feedback loop is increased, because the size of the loop is proportional to this gain.

In general, the stability of a feedback system is analysed by looking at the open loop response $Y_{cc} = \dot{w}_c / F_c$ through its Bode and Nyquist diagrams. This observation will allow us to know if the system is unconditionally stable, conditionally stable or unstable and to know the highest gain we can use without destabilising the system in case of conditional stability. We must take in account the whole range of frequencies here since the instabilities appear in the high frequencies even if the performances are expected in low ones.

Using the Bode diagram of the open loop transfer function we can observe the evolution of the phase of Y_{cc} so that we know if it stays between -90 and +90 degrees, if it is the case the system will be unconditionally stable, but if not, we will have to look at the Nyquist diagram to see if the system is unstable or conditionally stable.

In this work the sensor is considered an ideal system, thus the signal it produces is directly proportional to the velocity measured. Only the characteristics of the actuator have been taken in account so that the stability effects of the other components such as the accelerometer are not analysed.

Figure 3 shows the Bode diagram of the open loop sensor-actuator transfer function. The first thing to remark is that the response is characterised by well separated resonance in the low frequency, this is what we expected since it is those modes on which the control system must be effective. At higher frequencies the resonances are not so clearly separated because the natural frequencies become too close to each other, this is why the single feedback system cannot control the higher frequencies and thus limit the performance to the low ones.

The second thing that appears on the Bode diagram is that the phase remains between -90 and +90 degrees, thus the system is bound to be unconditionally stable.

In Figure 4 is presented the Nyquist diagram which confirms the system is unconditionally stable since the real part of the open loop transfer function remains positive. This result was expected since in this study the control force is collocated to the sensor so it cannot destabilise the system [23].

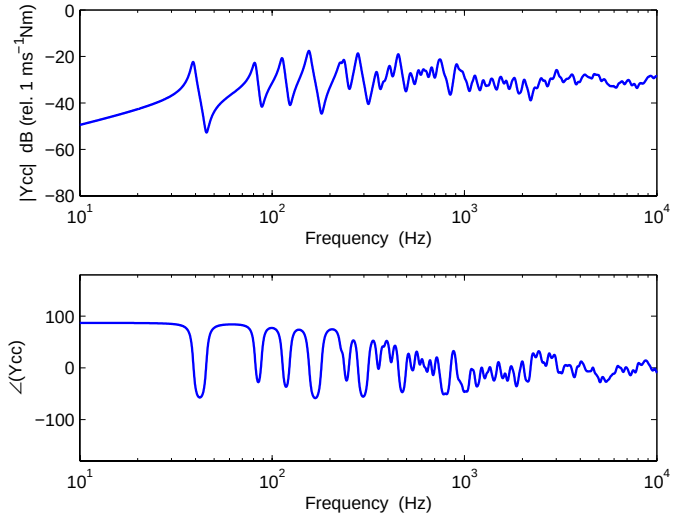

Figure 3: *Bode diagram of the transfer function of the open loop system* $Y_{cc} = \dot{w}_c / F_c$ *for a simply supported panel controlled by a single collocated force*

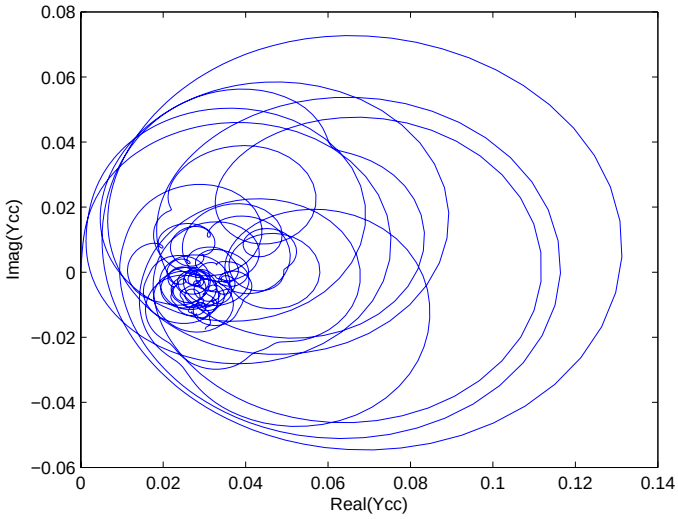

Figure 4: *Nyquist diagram of the open loop transfer function* $Y_{cc} = \dot{w}_c / F_c$ *for a simply supported panel controlled by a single collocated force*

2.3. Performance

The second issue we are interested to study is the control performances. In this case open loop sensor actuator response function is not sufficient to study the system's performance. To observe the system's performances at one point we study the closed loop control velocity $\dot{w}_c$ which is given by equation (8). This time it is sufficient to study the low frequencies since the control effects are expected only for the first few resonant modes.

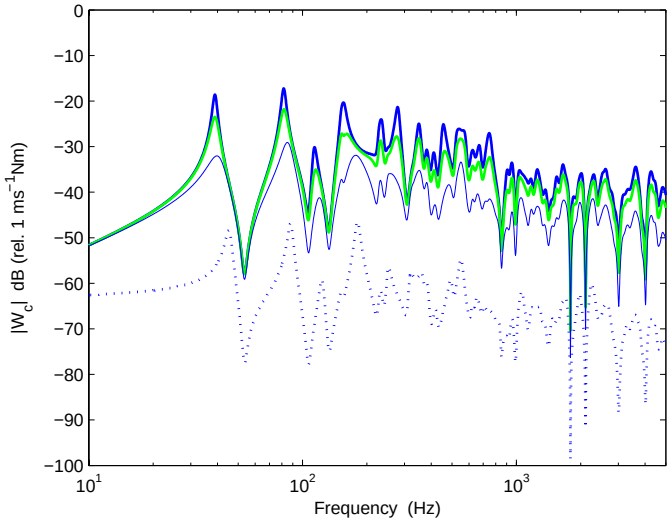

Figure 5: *Amplitude of the response to the control point for a simply supported panel, a single collocated force and some gain values* $g = 0$, $g = 10$, $g = 100$, $g = 10^6$ *(respectively thick black, grey, thin black, dotted)*

The plot in Figure 5 shows that up to 3 KHz, the dynamical behaviour is characterised by well-separated resonances like for the open loop sensor actuator response function, some of which are responsible for the transmitted sound. In this frequency range the modal overlap is very small, so that the panel's behaviour is only controlled by the resonant modes. Some of the modes do not have good radiation efficiency and do not transmit much sound; this is the case for the second and third mode for example.

Beyond this frequency range, the response of the panel is determined by the contribution of many modes that are overlapping. It is therefore very hard to distinguish the resonances at higher frequencies in the radiated power. In this frequency range, the radiated sound power is controlled by the mass of the panel.

The behaviour below 3 kHz is the one that interests us since by controlling the resonant modes it is possible to reduce the transmitted sound power.

Resonances can be controlled with active damping. In fact as we can see on Figure 5, the picks are lightened by the damping. That is why we use this active control to reduce radiated power. As the control gain is raised, the damping injected on the panel is increased and thus the resonance peaks are rounded off more and more (solid lines in Figure 5). However, when relatively larger control gains are implemented (dotted line in Figure 5) the picks are not lightened anymore, on the contrary the whole response drops out. This phenomenon comes from a structural change of the system. In fact the system tends to pin the panel at the control point [25]. The velocity of the control point is not representative anymore in this case.

The plot of Figure 5 represents the performance at on point, more precisely at the control point; in order to observe the performance on the entire panel we must plot the kinetic energy K of the panel. This quantity is given by the integral of the mass density time the thickness of the panel time the velocity over the surface of the panel and can be written in terms of the following modal summation:

$$K(\omega) = \frac{1}{2}\int_A \rho h \left|\dot{w}(x,y)\right|^2 dA = \frac{1}{4} M f_p^* \mathbf{a}_p^H \mathbf{a}_p f_p = \frac{1}{4} M f_p^* \left[\mathbf{a}_p + \mathbf{a}_{fc}\right]^H \left[\mathbf{a}_p + \mathbf{a}_{fc}\right] f_p \qquad (9)$$

with:

$$\mathbf{a}_c = \left[\begin{array}{c} \vdots \\ j\omega \dfrac{\phi_{m,n}(x_c, y_c)}{\Lambda[\omega_{m,n}^2(1 - j\eta_s) - \omega^2]} \\ \vdots \end{array}\right]_{m,n}, \qquad (10)$$

and

$$\mathbf{a}_{fc} = \mathbf{a}_c \frac{-g_c Y_{cp}}{1 + g_c Y_{cc}} \quad . \qquad (11)$$

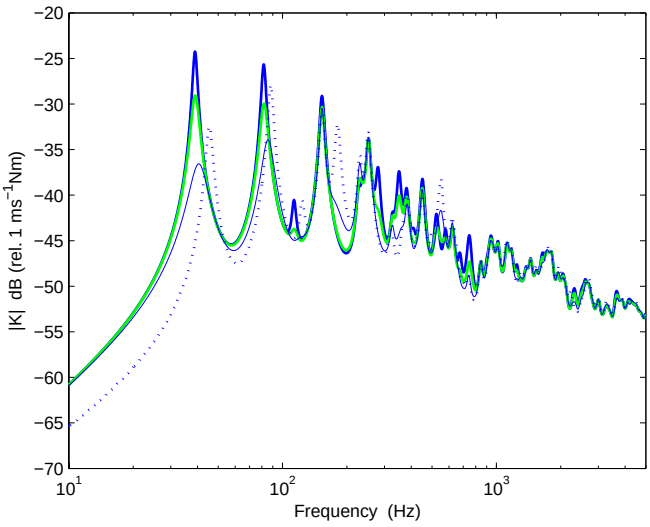

Figure 6: *Kinetic energy of a simply supported panel for a single collocated control force and the gain values:* $g = 0$, $g = 10$, $g = 100$, $g = 10^6$ *(respectively thick black, grey, thin black, dotted)*

Figure 6 shows that the kinetic energy of the panel decreases with increasing gain. As for the velocity the low frequencies picks are lightened as we increase the gain. It is interesting to note that for a very high value of gain a new resonance peak appears. This peak is due to a modification of the system mentioned above for high gains itself. This new resonance comes from the fact that the response of the simply supported panel has been changed to that of a simply supported panel which is also pinned at the control position. Thus the natural frequencies will not be the same as those of a

simply supported panel. When high control gains are implemented the control system does not efficiently control the global vibration of the panel.

It is therefore interesting to see for what gain we will have the best damping. To do so, we plot the ratio between kinetic energy with control on kinetic energy without control in function of the gain like shown in equation (9). This plot will show us the best gain necessary to have the lower energy level on the panel, i.e. the best control performance:

$$R = \frac{\int_0^\infty K_{fc}\, d\omega}{\int_0^\infty K_{nc}\, d\omega} \quad . \tag{12}$$

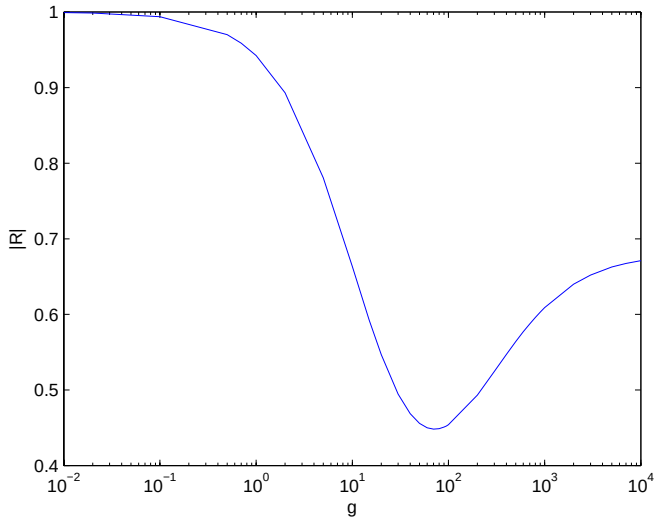

Figure 7: *Plot of the ratio R presenting the trim of the transmitted energy with control on transmitted energy without control function of the gain for a simply supported panel controlled by a single collocated force.*

Figure 7 shows that as the control gain is raised from zero, the kinetic energy of the panel goes down, as a result of the active damping action. However this trend is inverted for gains higher than 70 because the system does not produce active damping anymore since the panel has been pinned at the control position.

3. DIRECT VELOCITY FEEDBACK CONTROL LOOP ON A RESILIENTLY MOUNTED PLATE

3.1. Modelisation

The panel is not in practice simply supported neither clamped; we have to find an alternative modelisation of the mounting since the boundary conditions are of primary importance for the stability study of the feedback control loop. The idea to have a compromise between the clamped panel and the simply supported panel is to take a free panel and fix it to the frame with springs in translation and in rotation on its edges like presented in Figure 8.

Some indications of the boundary effects have been presented by Hong et al. [21] who has studied a feedback active control system on a resiliently mounted beam.

The number of springs used to simulate the mounting of the panel depends on the frequency range since the interval between two spring must be of the order of the quarter of the wave bending length in the panel so that the number of springs will be given by:

$$N = ceil\left(\frac{4 l_x f}{c}\right) = ceil\left(\frac{1}{\sqrt{\omega}}\sqrt[4]{\frac{B}{m}}\right) \quad , \tag{13}$$

with $B = EI$, $m = \rho h$ and c is the velocity of the flexural waves, f the frequency and l_x the length of the panel along the longest edge in x direction.

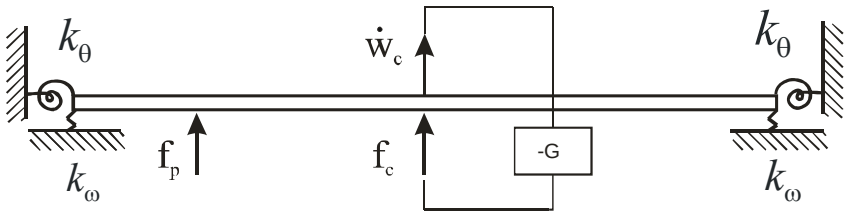

Figure 8: *transversal schema of a resiliently supported panel controlled by a single force collocated to the sensor*

In order to build a fully coupled model of the panel on flexible springs with the feedback control system, the velocities of each point of the panel's edge where we have a spring are ranged in a vector:

$$\dot{\mathbf{w}}_R = \begin{Bmatrix} \dot{w}_1 \\ .... \\ \dot{w}_R \end{Bmatrix} \quad . \tag{14}$$

The vibration at each of these mounting points is determined by the action of the primary force, the control force, and the force generated by its own springs and the ones of the other boundary points. The same effect occurs for the vibration at the control position which is determined by the action of the primary, control and boundary forces. Thus the response at boundary and control points can be expressed in terms of the following two matrix relations:

$$\dot{\mathbf{w}}_k = \mathbf{Y}_{kc} f_c + \mathbf{Y}_{kp} f_p + \mathbf{Y}_{kk} \mathbf{f} \tag{15}$$

$$\dot{w}_c = Y_{cc} f_c + Y_{cp} f_p + \mathbf{Y}_{ck} \mathbf{f}_k \tag{16}$$

where $\mathbf{Y}_{kc}$ is a matrix $2N \times 1$, $\mathbf{Y}_{ck}$ is a matrix $1 \times 2N$, $\mathbf{Y}_{kk}$ is a matrix $2N \times 2N$, $\mathbf{Y}_{kp}$ is a matrix $2N \times 1$ and $\mathbf{f}_k$ is the vector with the forces exerted by the linear and angular spring along the perimeter of the panel:

$$\mathbf{f}_k = \begin{Bmatrix} f_1 \\ .... \\ f_N \end{Bmatrix}.$$

The mobility functions in the matrices Y_{kk}, Y_{kc} and Y_{kp} are given by:

$$Y_{kc} = j\omega \sum_{m=1}^{\infty} \sum_{n=1}^{\infty} \frac{\phi_{m,n}(x_k, y_k) \phi_{m,n}(x_c, y_c)}{\Lambda[\omega_{m,n}^2 (1 - j\eta_s) - \omega^2]} \quad , \tag{17}$$

$$Y_{kp} = j\omega \sum_{m=1}^{\infty} \sum_{n=1}^{\infty} \frac{\phi_{m,n}(x_k, y_k) \phi_{m,n}(x_p, y_p)}{\Lambda[\omega_{m,n}^2 (1 - j\eta_s) - \omega^2]} \quad , \tag{18}$$

$$Y_{kk} = j\omega \sum_{m=1}^{\infty} \sum_{n=1}^{\infty} \frac{\phi_{m,n}(x_k, y_k) \phi_{m,n}(x_k, y_k)}{\Lambda[\omega_{m,n}^2 (1 - j\eta_s) - \omega^2]} \quad . \tag{19}$$

In this case the natural frequencies and natural modes are taken for a freely suspended panel. Thus according to reference, the natural frequencies are given by:

$$\omega_{m,n} = \sqrt{\frac{E_s h_s^2}{12 \rho_s (1 - \nu_s^2)}} \left(\frac{\pi}{l_x} \right)^2 q_{m,n}$$

with:

$$q_{m,n} = \sqrt{G_x^4(m) + G_y^4(n) (l_x / l_y)^4 + 2 (l_x / l_y)^2 \left[\nu H_x(m) H_y(n) + (1 - \nu) J_x(m) J_y(n) \right]} \tag{20}$$

and

1) for the even mode: $G_x = H_x = J_x = 0$

2) for the rocking mode: $G_x = H_x = 0$

$$J_x = \frac{12}{\pi^2}$$

3) for the first mode: $G_x = 1.506$

$$H_x = 1.248$$

$$J_x = 5.017$$

4) for the following modes: $G_x = m + \frac{1}{2}$

$$H_x = \left(m + \frac{1}{2}\right)^2 \left[1 - \frac{4}{(2m+1)\pi}\right]$$

$$J_x = \left(m + \frac{1}{2}\right)^2 \left[1 + \frac{12}{(2m+1)\pi}\right]$$

Also the natural modes are given by:

$$\phi_{m,n}(x,y) = \varphi_m(x)\varphi_n(y) \tag{21a}$$

where the beam functions $\varphi_m(x)$ and $\varphi_n(y)$ are given by:

$$\varphi_n = \begin{cases} \sqrt{2}\left\{\cos\left[\gamma_i\left(\frac{x}{l_x} - \frac{1}{2}\right)\right] + k_n \cosh\left[\gamma_i\left(\frac{x}{l_x} - \frac{1}{2}\right)\right]\right\}, \\ k_n = -\dfrac{\sin\left(\frac{1}{2}\gamma_i\right)}{\sinh\left(\frac{1}{2}\gamma_i\right)} \quad with \quad \tan\left(\frac{1}{2}\gamma_i\right) + \tanh\left(\frac{1}{2}\gamma_i\right) = 0 \\ for\ n\ unpair\ and\ i = \dfrac{(n+1)}{2} \\ \sqrt{2}\left\{\sin\left[\gamma_i\left(\frac{x}{l_x} - \frac{1}{2}\right)\right] + k_n \sinh\left[\gamma_i\left(\frac{x}{l_x} - \frac{1}{2}\right)\right]\right\}, \\ k_n = \dfrac{\sin\left(\frac{1}{2}\gamma_i\right)}{\sinh\left(\frac{1}{2}\gamma_i\right)} \quad with \quad \tan\left(\frac{1}{2}\gamma_i\right) - \tanh\left(\frac{1}{2}\gamma_i\right) = 0 \\ for\ n\ pair\ and\ i = \dfrac{n}{2} \end{cases} \tag{21b}$$

The forces exerted by the linear and angular springs f_k can be expressed in terms of the linear and angular velocities at the boundaries with the following matrix relation:

$$\mathbf{f}_k = -\mathbf{Z}\dot{\mathbf{w}}_k \tag{22}$$

where:

$$\mathbf{Z} = \begin{bmatrix} \mathbf{z}_w \mathbf{0} \\ \mathbf{0}\, \mathbf{z}_\theta \end{bmatrix} \tag{23}$$

is a $2N \times 2N$ matrix with

$$z_{wi} = \frac{k_w}{j\omega} \tag{24}$$

$$z_{\theta i} = \frac{k_\theta}{j\omega} \tag{25}$$

and k_w and k_θ are the stiffness in translation and in rotation of the springs respectively.

Thus substituting equation (22) into equation (15) after some mathematical manipulations, a response on the edges of the panel is found in term of the primary excitation and the control force:

$$\dot{\mathbf{w}}_k = \mathbf{T}_{kc} f_c + \mathbf{T}_{kp} f_p \tag{26}$$

with:

$$\mathbf{T}_{kc} = \left(\mathbf{I} + \mathbf{Y}_{kk}\mathbf{Z}\right)^{-1} \mathbf{Y}_{kc} \ , \tag{27}$$

$$\mathbf{T}_{kp} = \left(\mathbf{I} + \mathbf{Y}_{kk}\mathbf{Z}\right)^{-1} \mathbf{Y}_{kp} \ . \tag{28}$$

Thus substituting equation (26) into equation (16) the response at the control point is found to be:

$$\dot{w}_c = Q_{cc} f_c + Q_{cp} f_p \tag{29}$$

with:

$$Q_{cc} = Y_{cc} - \mathbf{Y}_{ck}\mathbf{Z}\mathbf{T}_{kc} \ , \tag{30}$$

$$Q_{cp} = Y_{cp} - \mathbf{Y}_{ck}\mathbf{Z}\mathbf{T}_{kc} \ . \tag{31}$$

The control force is still given by:

$$f_c = -g\dot{w}_c \ , \tag{32}$$

where g gain of the control system. Thus the response of the system at the control point will be:

$$\dot{w}_c = \frac{Q_{cp}}{1 + gQ_{cc}} f_p \quad . \tag{32}$$

In this report several cases of boundary stiffness are considered as listed in table 2 in order to study the response of the panel with reference to the stiffness of the mounting. The variation of the stiffness allows to simulate the comportment of the panel from a free panel to a clamped one or a simply supported one or to use intermediate values to simulate other mountings that better comply to real applications of smart panels.

Table 2: *several values of the stiffness in translation and in rotation for the different studies of chapter 2*

	k_w *[N/m]*	k_θ *[N/rad]*	panel
Case A	0	0	free
Case B	∞	0	Simply supported
Case C	∞	∞	clamped
Case D	10^{-1}	0	
Case E	10^{-1}	10^{-1}	

Since the system is not really clamped or simply supported, in order to modelise properly the system we must find the values of stiffness which give similar results to the experiments. Thus we have to test several values of stiffness and observe the system's response in these cases. The results are given in case C and D for a value of $k = 10^{-1}$ *[N/m] or [N/rad]*

3.2. Stability

The tools used to study the stability of each case in this section are the same as in the first chapter that is the Bode and the Nyquist diagram with reference to the Nyquist stability criterion. The panel studied is the same, only the boundary conditions are modified. For the stability we study here again the open loop sensor-actuator response function represented this time by the function $Q_{cc} = Y_{cc} - Y_{ck} Z T_{kc}$.

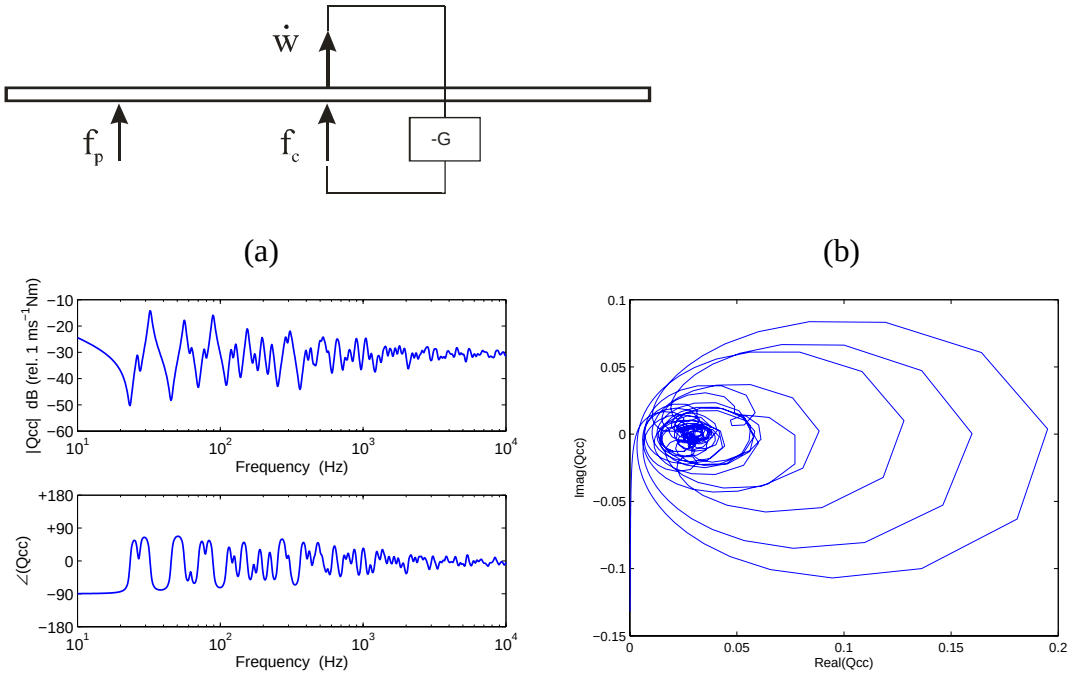

Figure 9: *Bode diagram (a) and Nyquist diagram (b) of the open loop transfer function* $Q_{cc} = \dot{w}_c / F_c$ *for a free panel controlled by a single collocated force.*

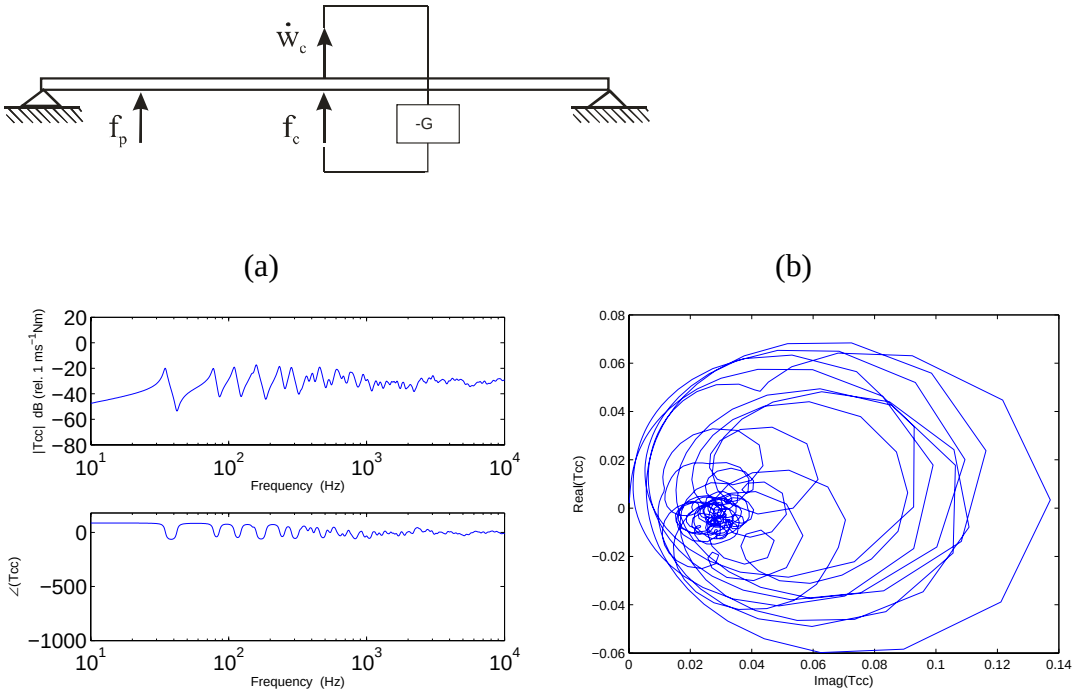

Figure 10: *Bode diagram (a) and Nyquist diagram (b) of the open diagram of the open loop transfer* $Q_{cc} = \dot{w}_c / F_c$ *for a resiliently supported panel with infinite stiffness in translation controlled by a single collocated force*

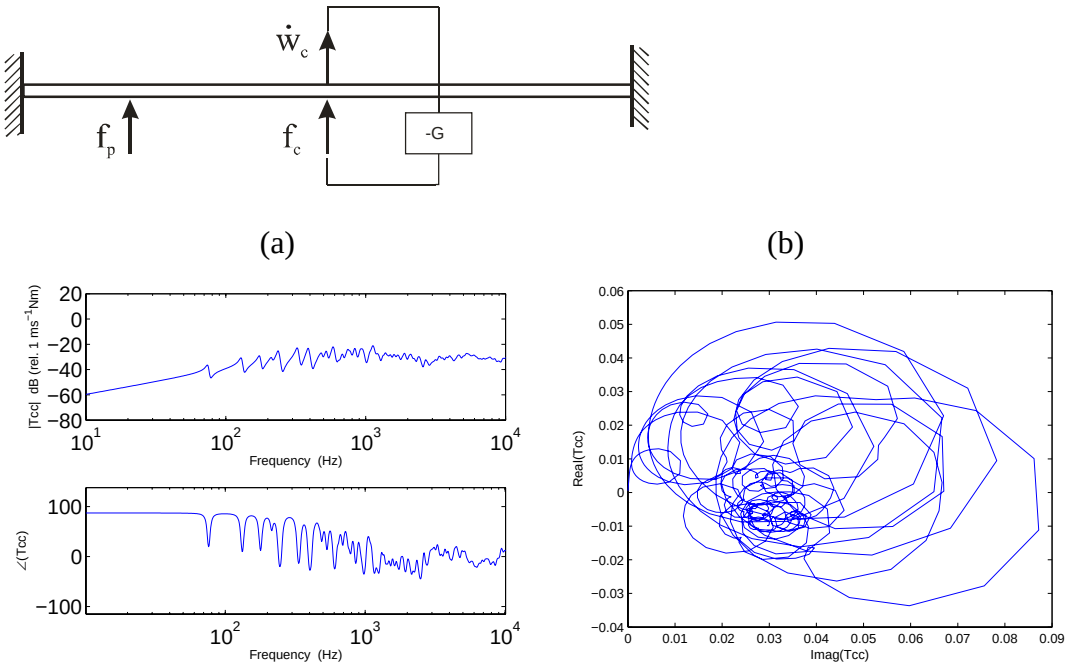

Figure 11: *Bode diagram (a) and Nyquist diagram (b) of the open loop transfer* $Q_{cc} = \dot{w}_c / F_c$ *for a resiliently supported panel with infinite stiffness in translation and in rotation controlled by a single collocated force.*

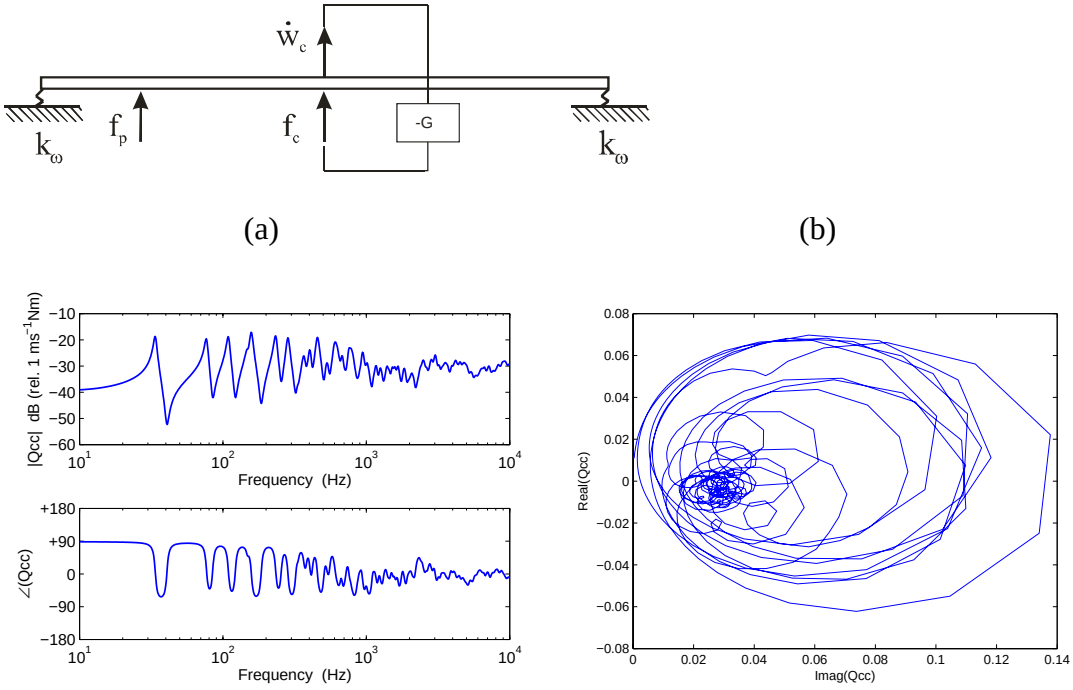

Figure 12: *Bode diagram (a) and Nyquist diagram (b) of the open loop transfer* $Q_{cc} = \dot{w}_c / F_c$ *for a resiliently supported panel with stiffness* $k = 10^{-1}$ *in translation controlled by a single collocated force.*

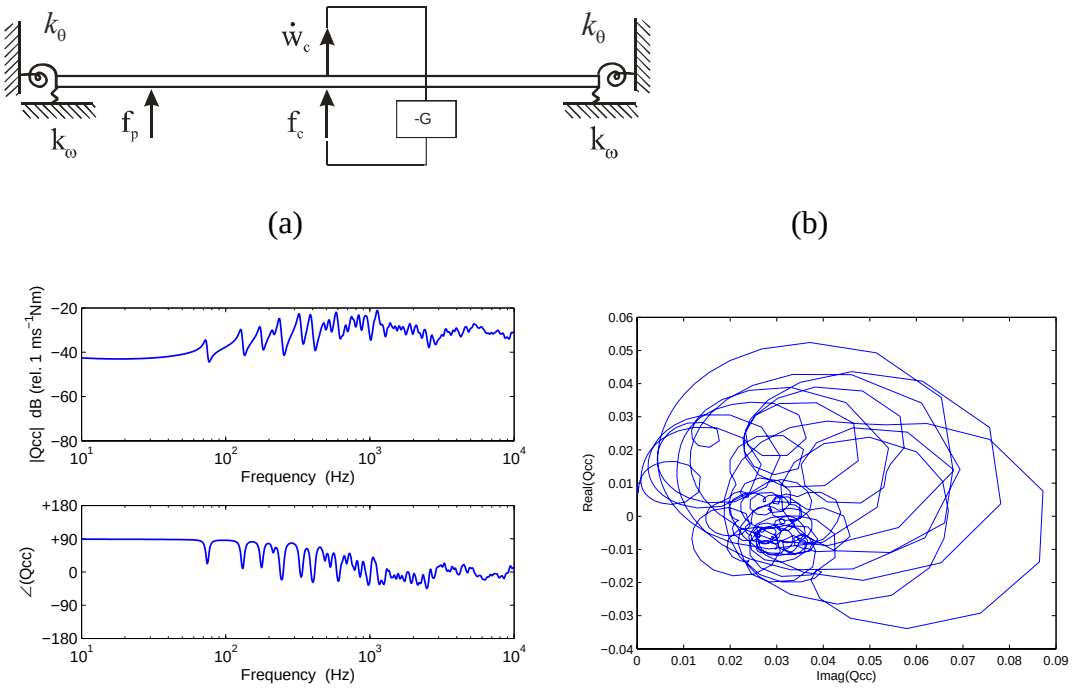

Figure 13: *Bode diagram (a) and Nyquist diagram (b) of the open loop transfer* $Q_{cc} = \dot{w}_c / F_c$ *for a resiliently supported panel with stiffness* $k = 10^{-1}$ *in translation and in rotation controlled by a single collocated force.*

In the case A of a free panel, on Figure 9a we observe an antiresonance in the low frequencies that is in fact the antiresonance of the first mode whose resonance is located at 0 Hz, (it is a rigid body mode). The profile of the diagram is then quite similar to the one obtained in the case of the simply supported panel with well separated resonances in the low frequencies and distance between the resonance frequencies which tend to decrease in the higher frequencies.

In case B for infinite stiffness as presented in Figure 10a as excepted we find the same results as for the simply supported panel which is normal since the panel is blocked in translation on its edge for infinite stiffness, the characteristics are therefore the same than for a simply supported panel.

The case C is equivalent to the case of a clamped panel. The panel is blocked in translation and in rotation. The plot in Figure 11a shows that resonances appear for a higher frequency than for the simply supported panel and the plot starts with smaller amplitude at low frequency to finally reach the same level than for the case B.

In case D the plot in Figure 12a shows that in the case of a panel supported by stiffness in translation non infinite, the first resonance does not appear at the same frequency than for the simply supported but since the panel is not free, it is not located on 0 Hz. In fact the frequency of the first resonance will depend on the value of the stiffness and will be located between 0 Hz and the frequency of the first resonance for a simply supported panel (35 Hz for the panel of our study). At very low frequencies before the first resonance, the slope of the modulus of the open loop sensor-actuator response function also depends on the stiffness of the springs along the panel's edge; it increases from the slope for a free panel to the slope for a simply supported one with the stiffness.

The effect of the rotational springs will be the same; the panel properties will go from the ones of a simply supported panel to the ones of a clamped panel as the rotational stiffness increase. As shown Figure 13a, This implies that when the rotational stiffness increase, the value of the frequency for the first resonance increase so as the slope before this resonance while the amplitude in very low frequencies goes down.

Figures 9a-13a also represent the phase of the open loop sensor actuator response function, the phase remains between -90 and +90 degrees so that the system is unconditionally stable. This result is confirmed by Figures 9b-13b that represent the Nyquist plots of these functions. The real part of the open loop open loop sensor actuator functions never turns to be negative, the system is thus unconditionally stable.

It is important to note that the values of stiffness considered in this study are much smaller than the ones which should be used to modelise the panel's mounting in reality, this allows to see the phenomena more clearly to analyse them in this section.

3.3. Performance

In this section, the performances of the feedback control loop for several stiffness of the mounting system are analysed. In order to do so, the velocity at the control point and the kinetic energy of the panel are plotted for each mounting case so that the response of the control point and the global panel response can be analysed.

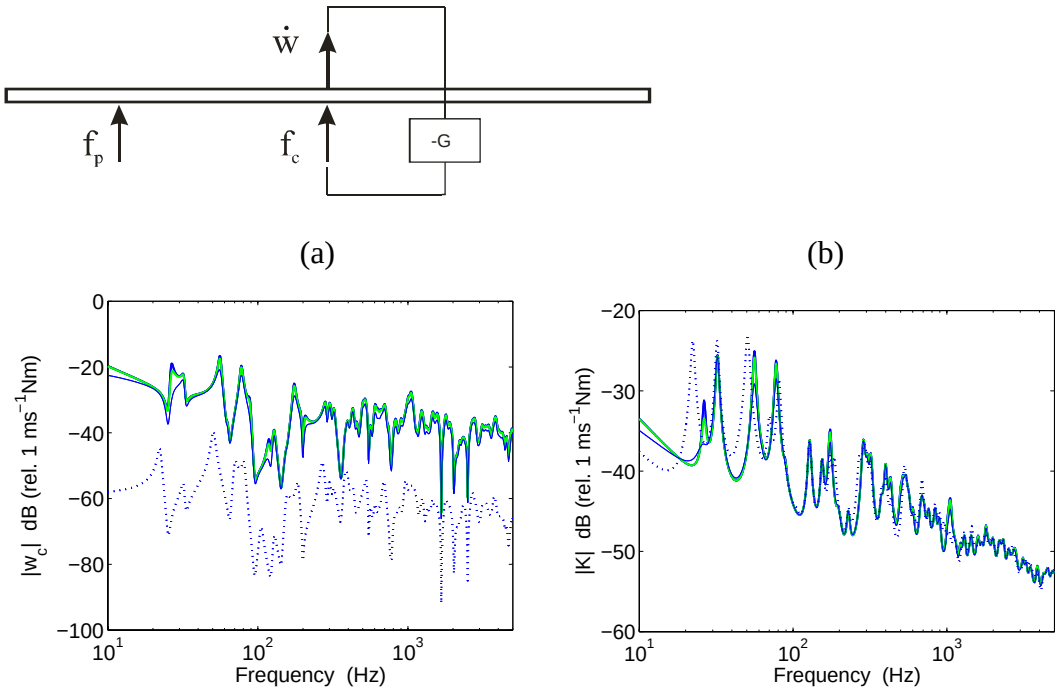

Figure 14: *Amplitude of the response at the control point (a) and kinetic energy of the panel (b) for a free panel controlled by a single collocated force and some gain values:* $g = 0$, $g = 10$, $g = 100$, $g = 10^6$ *(respectively thick black, grey, thin black, dotted)*

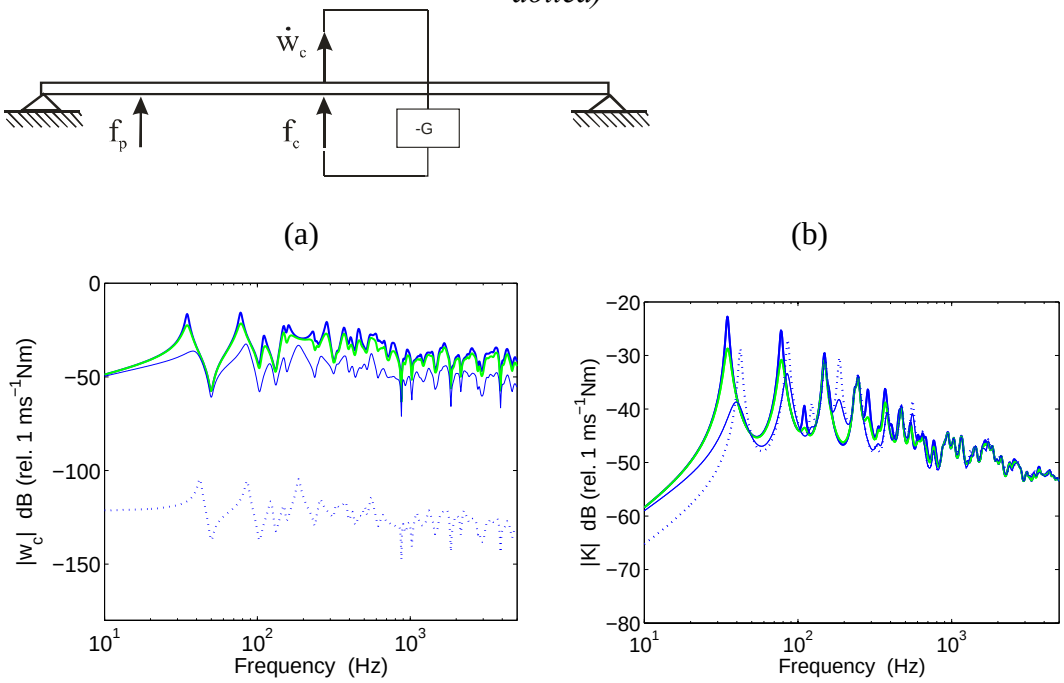

Figure 15: *Amplitude of the response to the control point (a) and kinetic energy of the panel (b) for a resiliently supported panel with infinite stiffness in translation controlled by a single collocated force and some values of gain:* $g = 0$, $g = 10$, $g = 100$, $g = 10^6$ *(respectively thick black, grey, thin black, dotted)*

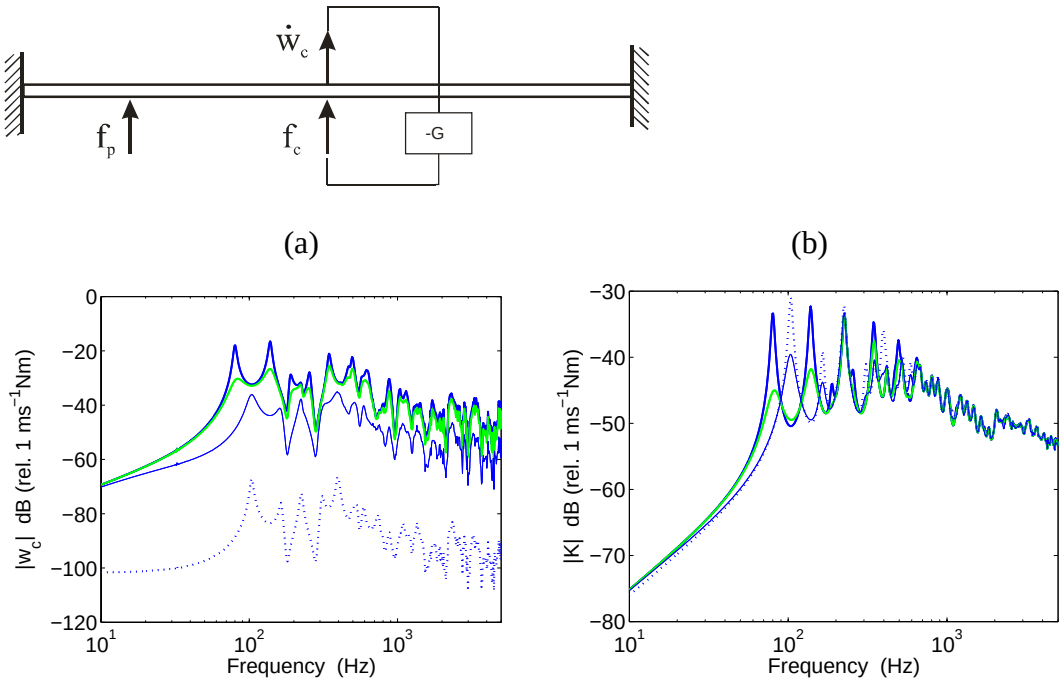

Figure 16: *Amplitude of the response to the control point (a) and kinetic energy of the panel (b) for a resiliently supported panel with an infinite stiffness in translation and in rotation controlled by a single collocated force and some values of gain* $g = 0,\ g = 10,\ g = 100,\ g = 10^6$ *(respectively thick black, grey, thin black, dotted)*

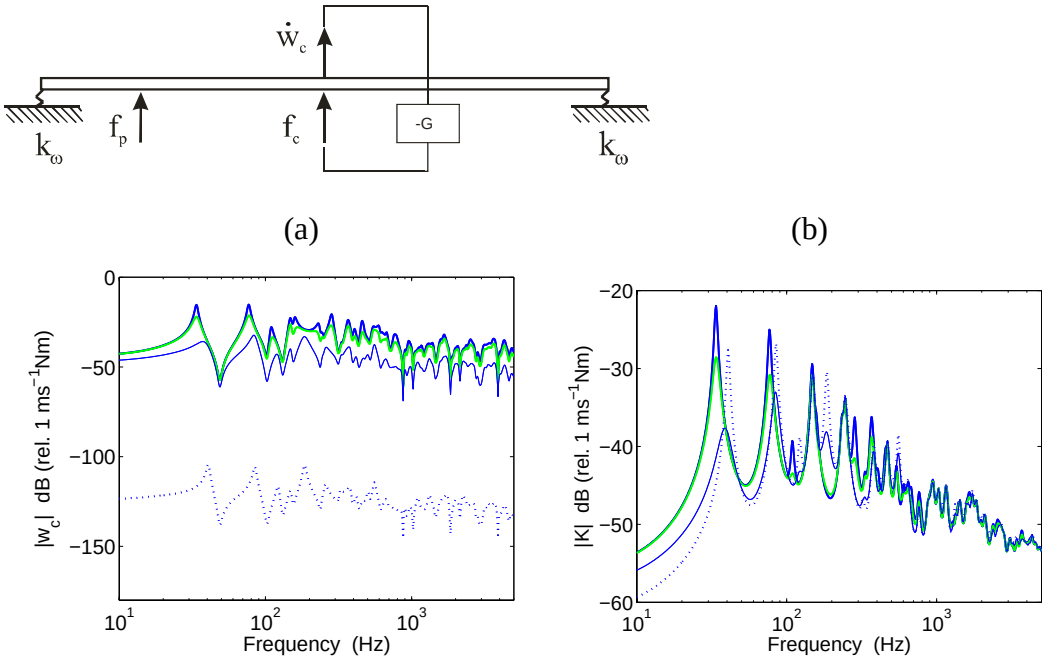

Figure 17: *Amplitude of the response to the control point (a) and kinetic energy of the panel (b) for a resiliently supported panel with a stiffness* $k = 10^{-1}$ *in translation controlled by a single collocated force and some gain values:* $g = 0,\ g = 10,\ g = 100,\ g = 10^6$ *(respectively thick black, grey, thin black, dotted)*

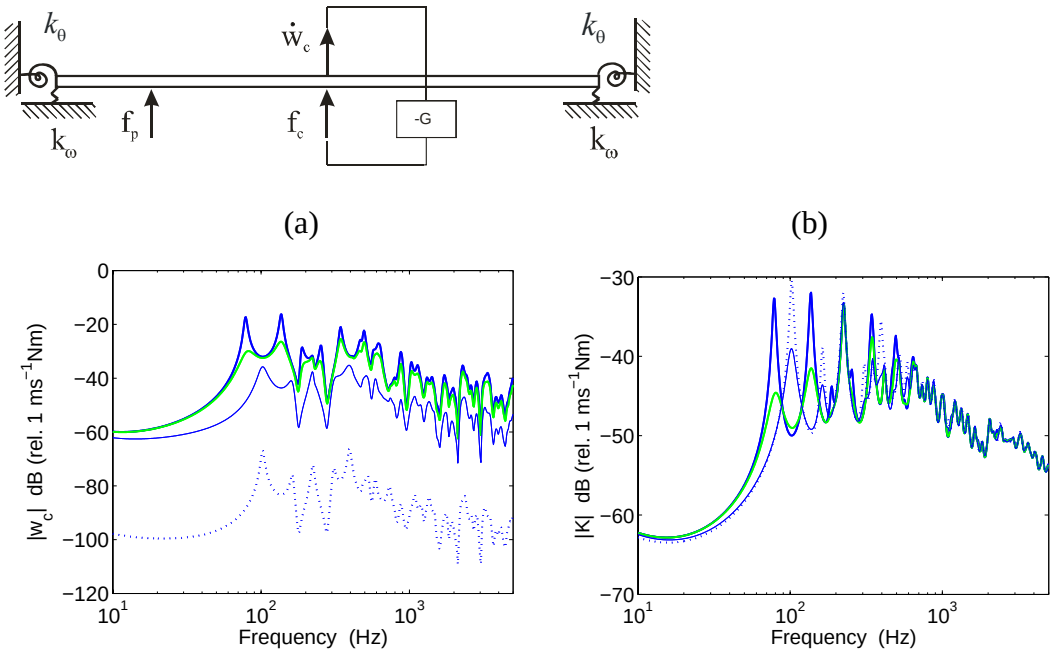

Figure 18: *Amplitude of the response to the control point (a) and kinetic energy of the panel (b) for a resiliently supported panel with a stiffness* $k = 10^{-1}$ *in translation and in rotation controlled by a single collocated force and some values of gain*: $g = 0$, $g = 10$, $g = 100$, $g = 10^6$ *(respectively thick black, grey, thin black, dotted)*

For the case A, on Figure 14a we have an anti resonance in the low frequencies without any resonance before on the plot. The first resonance is here again at 0 Hz for the rigid body mode of the freely suspended panel so that only the antiresonance appears on the plot. We can note that the curve is notably modified for high gain values (doted line); this phenomenon is due to the change of the system studied. For very high gains, the system becomes a pinned panel at the control point so that the first resonance is moved up in frequency as it appears on the plot. But this last case is to avoid since the control is not efficient anymore.

This modification of the system is also visible on the Figure 14b which represents the kinetic energy. For very high gain values (dotted line) new resonance picks of resonance appear; the system is not efficient for this gain values. Kinetic energy also decrease starting from 0 Hz since the panel is free.

In case B we only have a spring in translation with an infinite stiffness, this case correspond to a simply supported panel. The plots Figure 15 have therefore the same shapes as those found in section 1.3. and we find again the same control properties for high gain values.

The same phenomenon as for the case A (free panel) appears for a gain too high in the other cases (simply supported panel, clamped panel end resiliently mounted panel); the panel becomes too stiff at the control point and the system is modified.

The kinetic energy in Figure 17b presents the same profile as the one of a simply supported panel with the same characteristics except the slope is smaller in the low frequencies. This is the result of the choice of the stiffness and the slope will depend on its value.

The slope of the panel's kinetic energy is again changed in case D for the closed loop as for the open loop the slope is function of the stiffness in rotation and in translation. We therefore have two control levers to act on the system, one in rotation

and one in translation. We can, thanks to these levers modelise precisely the boundary condition of the panel to study its stability.

More generally from Figures 14a,b to 18a,b we can note for all cases A to E that:

1) as the control is increased the resonance peaks are lightened until the pinning effect changes the structure properties of the system.
2) this phenomenon is more pronounced in the lower frequencies where we expect the control system to be efficient
3) the damping is most efficient in the case of the clamped panel

Since for the control system mounted on a resiliently supported panel the same type of control behaviour has been observed as for the control system mounted on the simply supported panel we shall plot the ratio *R* in order to check if we can find the optimum value of gain to have the less energy transmitted possible.

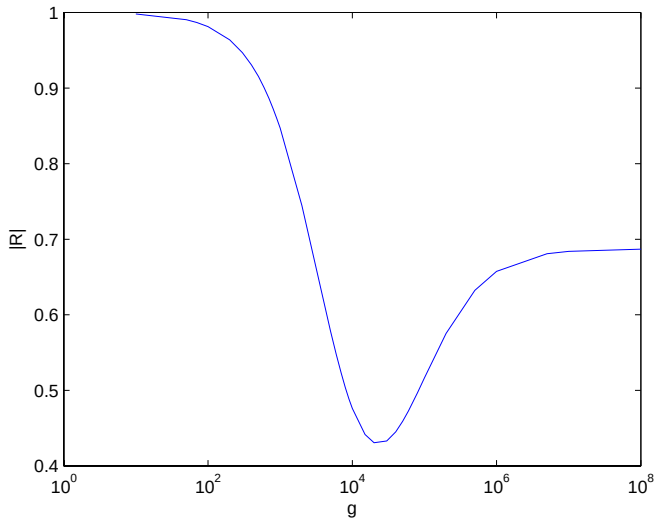

Figure 19: *Plot of the ratio R presenting the trim of the transmitted energy with control on transmitted energy without control function of the gain for a resiliently supported panel with stiffness* $k = 10^{-1}$ *in translation controlled by a single collocated force.*

Figure 19 present the same shape for the ratio *R* than for the simply supported panel so that for each value of stiffness we will have to find the best gain in order to have an optimal control on the panel.

4. DIRECT VELOCITY FEEDBACK USING TRIANGULARLY SHAPED ACTUATORS

The third part of this study focuses on the response of a resiliently supported panel controlled by 16 triangular piezoelectric actuators evenly distributed along the edge of the panel as presented in the Figure 20. Recently analytical and experimental studies have been developed to control structural vibration and sound radiation from flat panel using 16 square piezoelectric actuators and accelerometer sensors pairs [18]. Each sensor-actuator pair is used to implement a decentralized direct velocity feedback control loop. Single-sided piezoelectric actuator provides the structural control inputs while the closely located sensor is used as error signals. These 16 independent feedback loops synthesize point damping, which efficiently reduce the vibration and sound radiation of low frequency resonances of the panel. Thus, the control of far field sound pressure has been achieved by introducing additional active damping to the structure.

The smart panel with square patch actuator is used to generate “surface active damping”, and this new type of smart panel generates “boundary active damping”. Although a previous theoretical study has shown only a small advantage of boundary active damping compared to surface active damping, the arrangement acting along the boundary of the panel has great advantage in that it is not invasive. Thus this configuration can be used in a wider class of application including glasses of the transportation vehicles, for example.

The sensor is localised at the top of the triangles. Each control unit acts like a skyhook damper like presented in the Figure 21, so that the system tends to create anechoic boundary conditions that reduce reflection of waves and as consequence of the creation of resonating modes. The triangular actuators are made of a piezoelectric PZT ceramic, which are well adapted to active control systems since they are able to produce relatively strong bending stresses when bonded to a system.

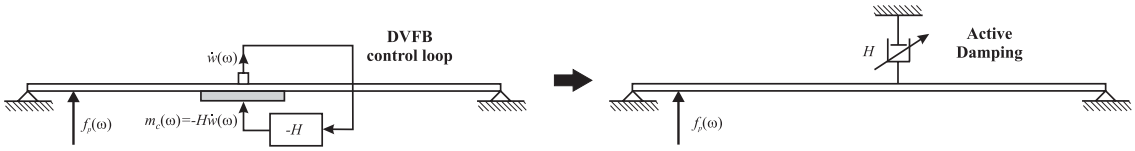

Figure 20: *Transversal schema of the active damping and its equivalence with the skyhook system.*

Each actuator generates a force at its top which is collocated with the sensor but also bending moments along its three edges and also two single forces at the angle of the bases due to the fact the actuator is not perfectly aligned to the border of the panel. These excitation components are presented Figure 22. The excitations non collocated to the sensor will tend to destabilise the system. Therefore it will be necessary to observe the open loop of the system to know whether the system is unconditionally stable, unstable or conditionally stable, and in this last case what is the maximum gain we can apply in order to have the best stable response. The stability will also depend on the border conditions and therefore on the stiffness of the springs

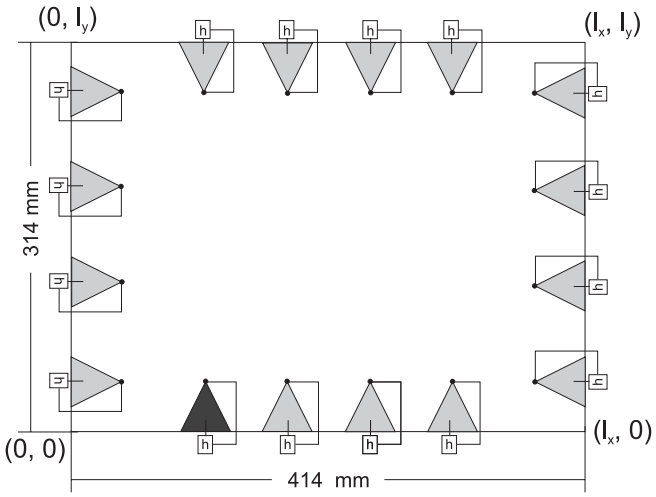

Figure 21: *Panel with 16 triangular piezoelectric actuator*

The system is a decentralised control system, that is each control loop, and therefore each actuator, is working independently from the others. In other term the control force produced by the actuator is only dependent on the signal measured at the top of the triangle.

The characteristics of the piezoelectric actuator and the properties of the ceramic material are summarized in table 3:

In this chapter we focus our attention on the stability and control performance of one of the sixteen decentralised control unit.

Table 3: *physical and material properties of the piezoelectric actuator*

Parameter	**Value**
Material	$Pz27$
Base and height	$b \times a = 40 \times 40mm$
Thickness	$h_{PZT} = 5mm$
Density	$\rho_{PZT} = 7600kg/m^3$
Young's modulus	$E_{PZT} = 6.3 \times 10^{10} N/m^2$
Poisson ratio	$\nu_{PZT} = 0.29$
PZT strain/charge constants	$d_{31}^0 = 166 \times 10^{-12} m/V$ $d_{32}^0 = 166 \times 10^{-12} m/V$ $d_{31}^0 = 0m/V$

4.1. Modelisation

The transfer function *Ycc* between the velocity at the tip of the actuator and the input to the piezoelectric patch is changed in order to take in account the several effects of the piezoelectric actuator, bending moments and forces. The new expression is given by:

$$Y_{cc} = j\omega \sum_{m=1}^{\infty}\sum_{n=1}^{\infty} \frac{\phi_{m,n}(x_c, y_c) F_{m,n}}{\Lambda\left[\omega_{m,n}^2 (1 - j\eta_s) - \omega^2\right]} \quad , \tag{33}$$

with [18]:

$$F_{m,n} = \frac{h_s}{2}\left(m^2 e_{31}^0 + e_{32}^0\right)\left\{\int_{vs1}^{vs3} \frac{\partial \Phi_{m,n}(x,y)}{\partial n_{ls1}} dl_{s1} + \int_{vs2}^{vs3} \frac{\partial \Phi_{m,n}(x,y)}{\partial n_{ls2}} dl_{s2}\right\} + \frac{h_s}{2} e_{31}^0 \int_{vs1}^{vs2} \frac{\partial \Phi_{m,n}(x,y)}{\partial n_{bs}} db_s$$
$$+ 4\frac{h_s}{2} m e_{31}^0 \Phi_{m,n}(x_{vs3}, y_{vs3}) - 2\frac{h_s}{2} m e_{31}^0 \left(\Phi_{m,n}(x_{vs1}, y_{vs1}) + \Phi_{m,n}(x_{vs2}, y_{vs2})\right) \tag{34}$$

We should point out here that the excitation components of the piezoelectric actuator do not have the same importance since they are moderated by the characteristics of the actuator as shown in Figure 22. The three first terms represent the bending moments on the left edge, the right edge and the base edge, respectively. The fourth term represents the force at the tip of the actuator which is the most important in amplitude and the one which interests us since it is collocated and dual with the velocity sensor and thus should guarantee relatively high stability and control performance. The two last terms represent the forces at the corner of the base of the actuator which can destabilise the system since they are not collocated with the sensor. Their amplitude is less important than the top force but a high gain can make them important enough to destabilise the system.

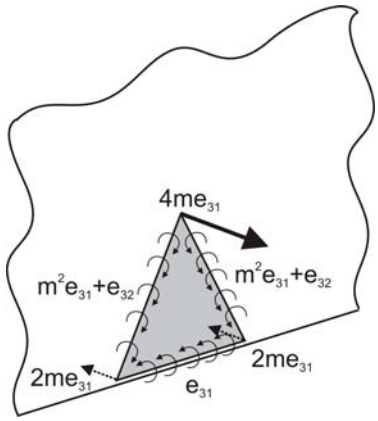

Figure 22*: schema of the triangular piezoelectric actuator and its several actions.*

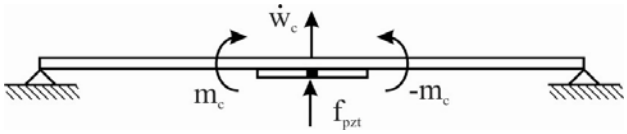

Figure 23: *transversal schema of the piezoelectric actuator stick on the panel and its moment effects.*

Table 4: *several values of the stiffness in translation and in rotation for the different studies of chapter 3*

	k_w	k_θ
Case A	0	0
Case B	∞	0
Case C	∞	∞
Case D	10^{-2}	0
Case E	10^{-2}	10^{-2}

4.2. Stability

The study of the stability in this chapter is still based on the Bode and Nyquist diagram. As discussed above the excitation components are not all collocated to the sensor so we may have instabilities. It will also be interesting to study each excitation components of the actuator in order to know which of them have the most destabilising effect and in which frequencies its effect is relevant.

The results presented in Figures 24a,b to 28a, bare for the cases (A-E) of mounting stiffness for a control point at the top of the first triangular actuator starting from the corner (back actuator Figure 21).

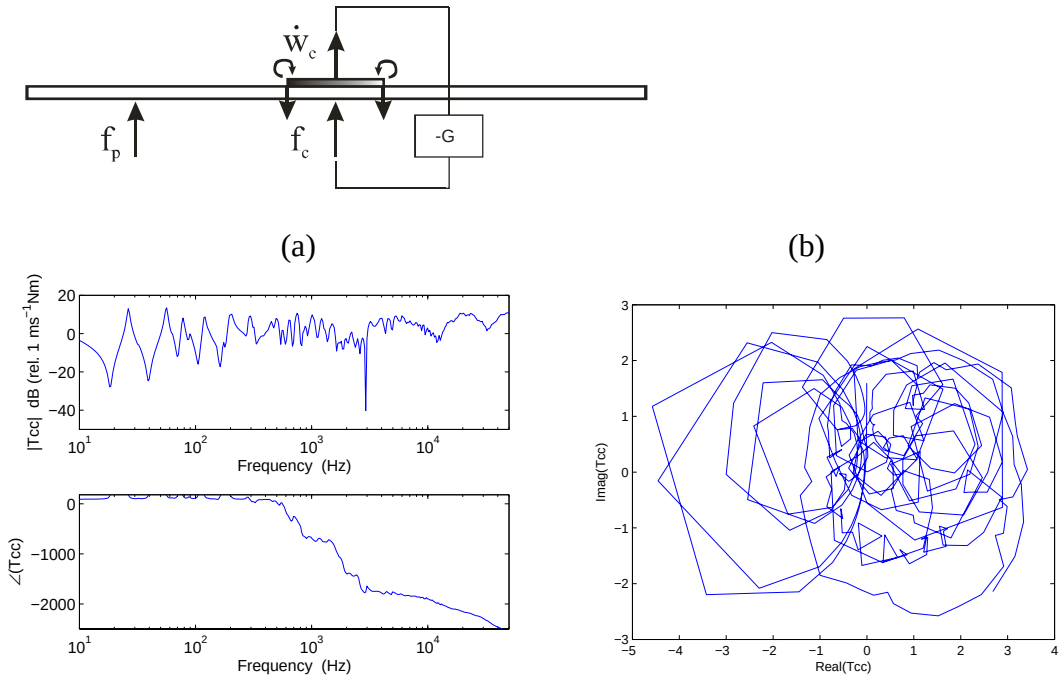

Figure 24: *Bode diagram (a) and Nyquist diagram (b) of the open loop transfer function for a free panel controlled by a triangular piezoelectric actuator.*

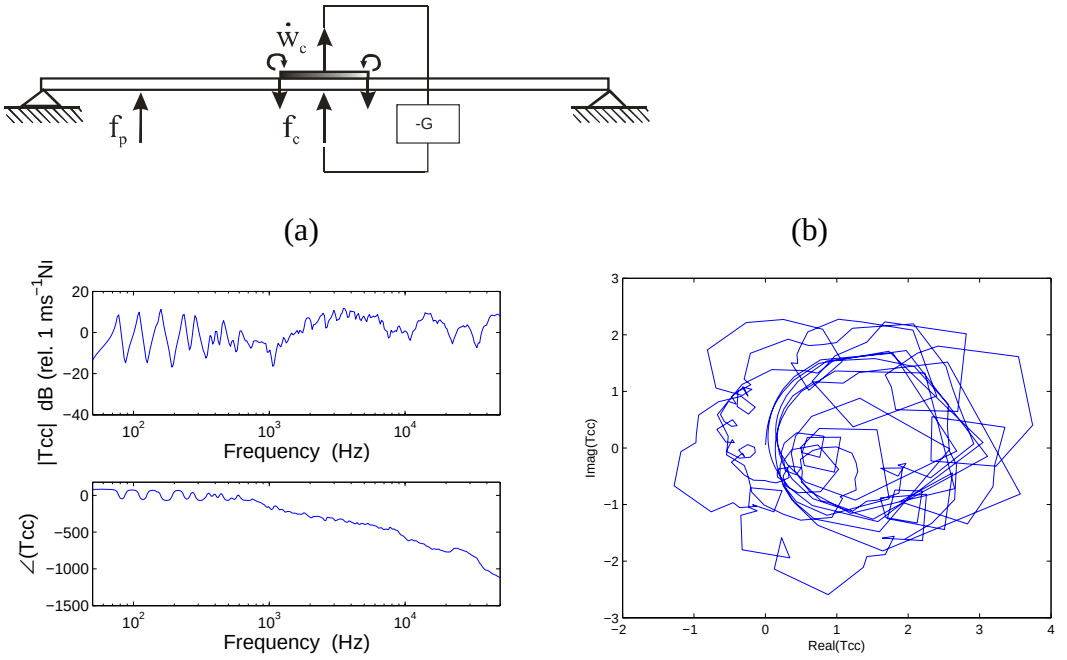

Figure 25: : *Bode diagram (a) and Nyquist diagram (b) of the open loop transfer function for a resiliently supported panel controlled by a triangular piezoelectric actuator for an infinite stiffness in translation.*

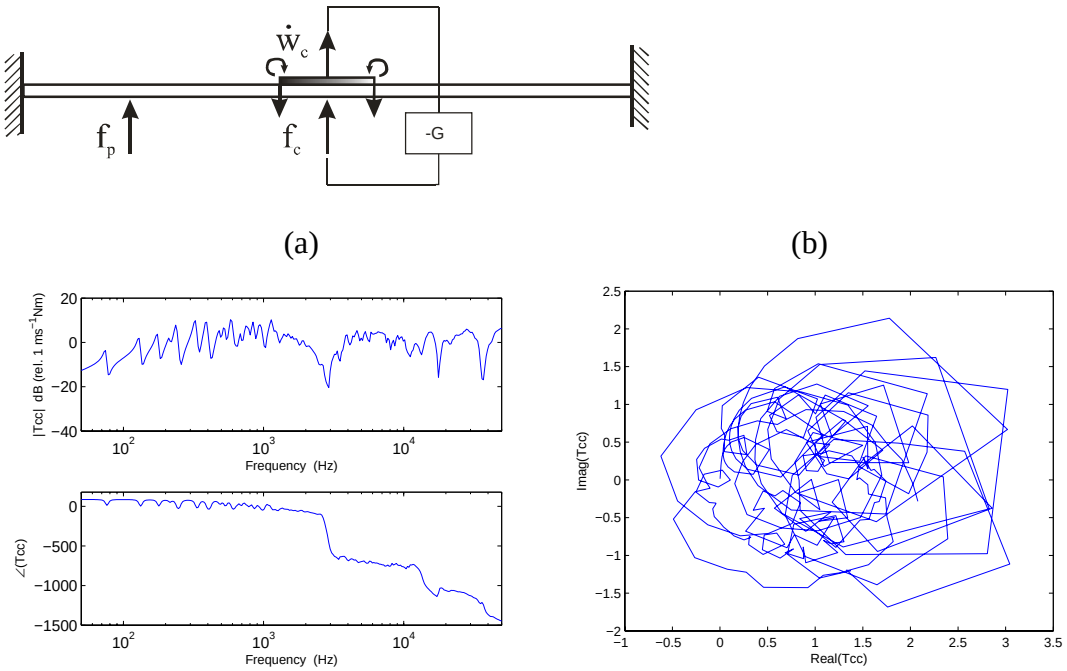

Figure 26: : *Bode diagram (a) and Nyquist diagram (b) of the open loop transfer function for a resiliently supported panel controlled by a triangular piezoelectric actuator for an infinite stiffness in translation and in rotation.*

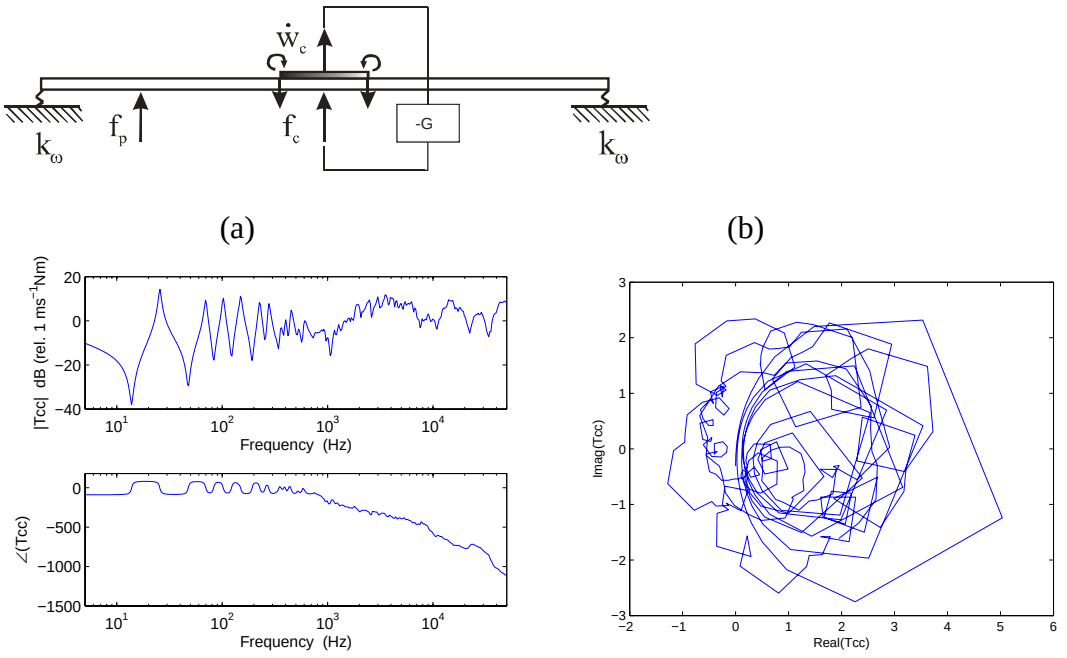

Figure 27: : *Bode diagram (a) and Nyquist diagram (b) of the open loop transfer function for a resiliently supported panel controlled by a triangular piezoelectric actuator for stiffness of $k=10^{-2}$ in translation.*

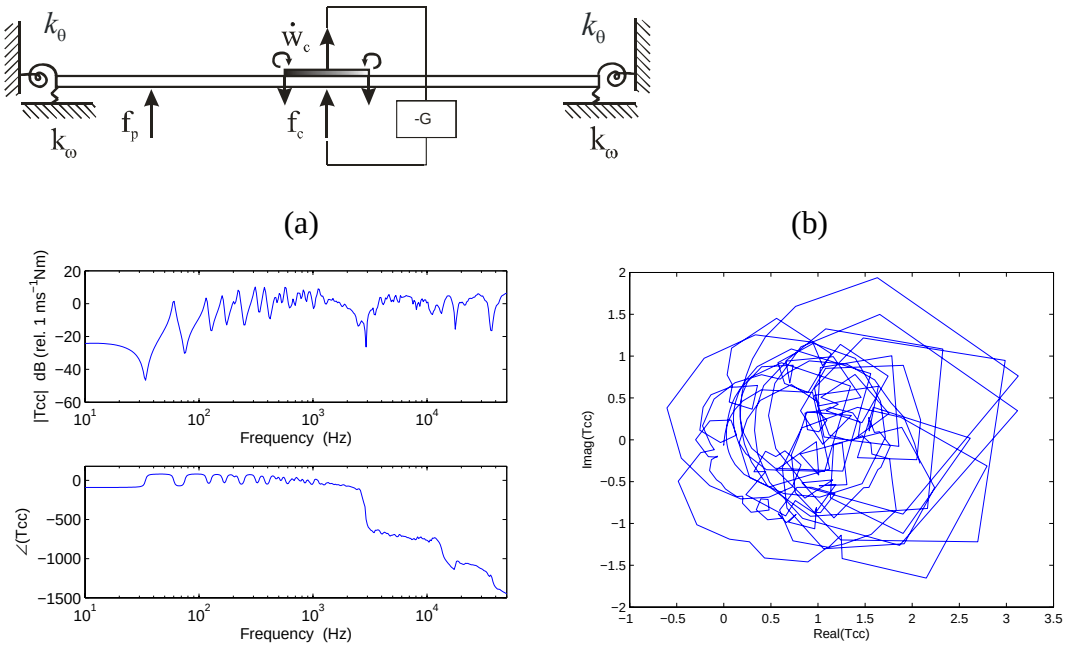

Figure 28: : *Bode diagram (a) and Nyquist diagram (b) of the open loop transfer function for a resiliently supported panel controlled by a triangular piezoelectric actuator for stiffness of* $k=10^{-2}$ *in translation and in rotation.*

The first remarkable thing on Figures 24a to 28a is that at low frequencies, the phase of the triangular actuator is situated between -90 and +90 degrees, this means the system remains stable in this frequency range but the phase decreases for high frequencies. Therefore the system can turn unstable; we will have to study the Nyquist plot of the open loop transfer to judge the stability of the system.

The amplitude of the response of the triangular piezoelectric actuator shown in Figures 24a to 28a have a lot of similarities with the equivalent amplitudes shown in Figure 9a to 13a that represent the response at the control point for a single force. However there is a notable difference between these figures. Drops in the amplitude appear in high frequencies for the triangular shaped actuator. These drops are a peculiarity of the triangular shape. They are due to the cancellation effect of the different stresses produced by the actuator. Because these different stresses are not applied at the same location, their effect at the sensor's position is seen with a phase lag, which leads to interferences that can reduce the amplitude of the response. This phase lag can be easily evaluated, knowing that the velocity of flexural is given by:

$$c_b = \sqrt{2\pi f}\sqrt[4]{\frac{Eh^2}{12\left(1-\nu^2\right)\rho}},$$

where f is the frequency, E the Young modulus, ν the Poisson's coefficient, ρ the density and h the thickness of the plate.

Since the bending wavelength is given by:

$$\lambda = \frac{c_b}{f}$$

then $$\lambda = \frac{3.13}{\sqrt{f}} \quad .$$

Therefore the phase lag created by a distance d is equal to:

$$\varphi = -\frac{2\pi h}{\lambda} = -\frac{2\pi h\sqrt{f}}{3.13} .$$

The first resonance frequencies are also not the same for the case B to E; this comes from the value of stiffness chosen for the simulation. As said in the second chapter, the frequency of the resonance picks depend on the value of the stiffness which as been chosen differently in this chapter to observe clearly the influence of these of the mounting stiffness on the stability and thus control performance.

The analysis of the Nyquist diagram confirms that the system is not unconditionally stable anymore and could turn unstable for high gain values. The cases do not present also the same margin gain. For the case A where the panel is free, the point (-1, 0) is enclosed on Figure 24b, the system becomes unstable. This is due to the fact the panel is not fixed at all. As the transversal stiffness is increased the real part of the open loop transfer function of the system goes less in the negative parts of the plot (Figures 10b and 12b). The same phenomenon is observed when we increase the rotational stiffness (Figures 11b and 13b), so that the most stable case is found to be the case C of the clamped panel. The stiffness of the mounting appears to be a key element for the stability of the system. It is to note on Figure 27b that the real part of the open loop transfer function goes very much in the negative values, this is due to the fact the panel is fixed to the frame by springs with very small stiffness so that it remains quite free. In real application the stiffness is normally much more effective so that the open loop transfer does not go as much in the negative values.

The Bode diagrams of the sensor-actuator frequency response function of each component of the actuation (point forces at the corner and moments along three edges) have been plotted in Figure 29 to analyse their effect on global response. Only the case of the simply supported panel is presented here, since the conclusions are similar for the other cases.

The phase of the response due to the point force remains between -90 and +90 degrees; this force does not bring any instability since it is collocated with the sensor. The amplitude of the response due to the moment along the edge keeps increasing, whereas the phase goes down at high frequencies. This phenomenon is very harmful for the stability because it means that the amplitude at the frequencies where instability phenomena can occur is relatively high.

The phase due to the moments of the two other edges and the ones due to the forces on the corner at the base of the triangle also goes down at high frequencies. But the amplitude at high frequencies is much lower than the amplitude due to the moment on the base. Therefore these excitation components might bring instabilities as well, although their effect is not as important as for the base moment.

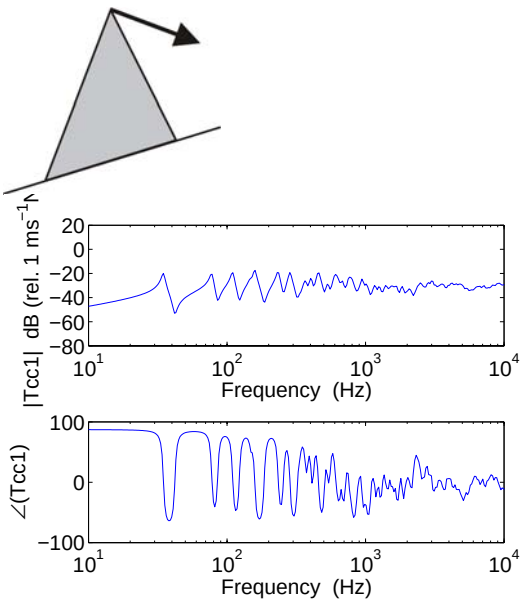

a. Single force at the top of the actuator .

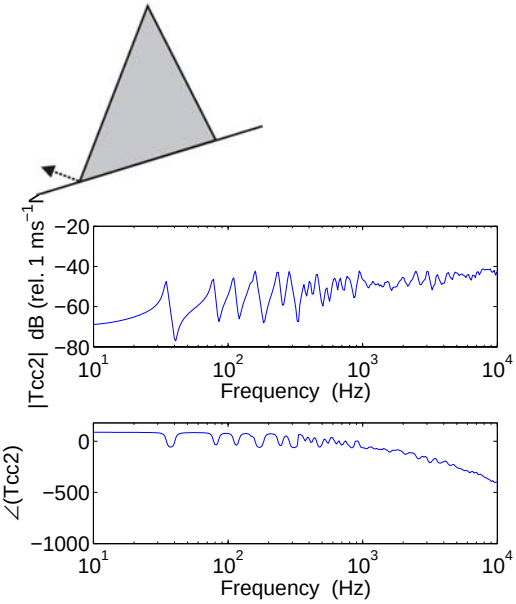

b. Single force at the left angle of the actuator

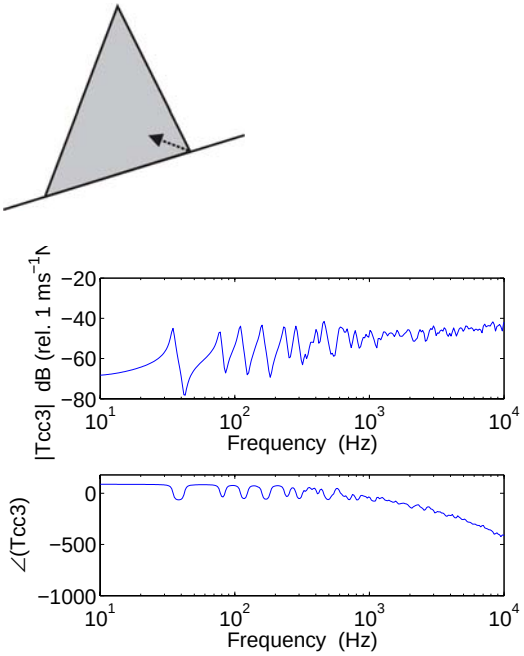

c. Single force at the right angle of the actuator

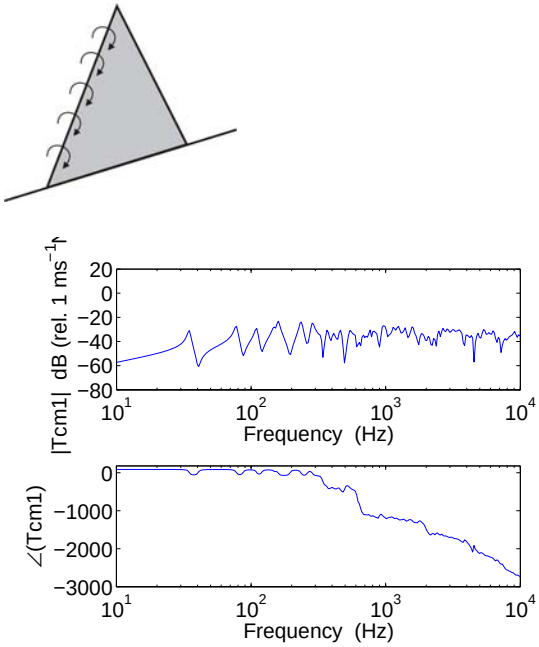

d. Bending moment on the left edge of the actuator

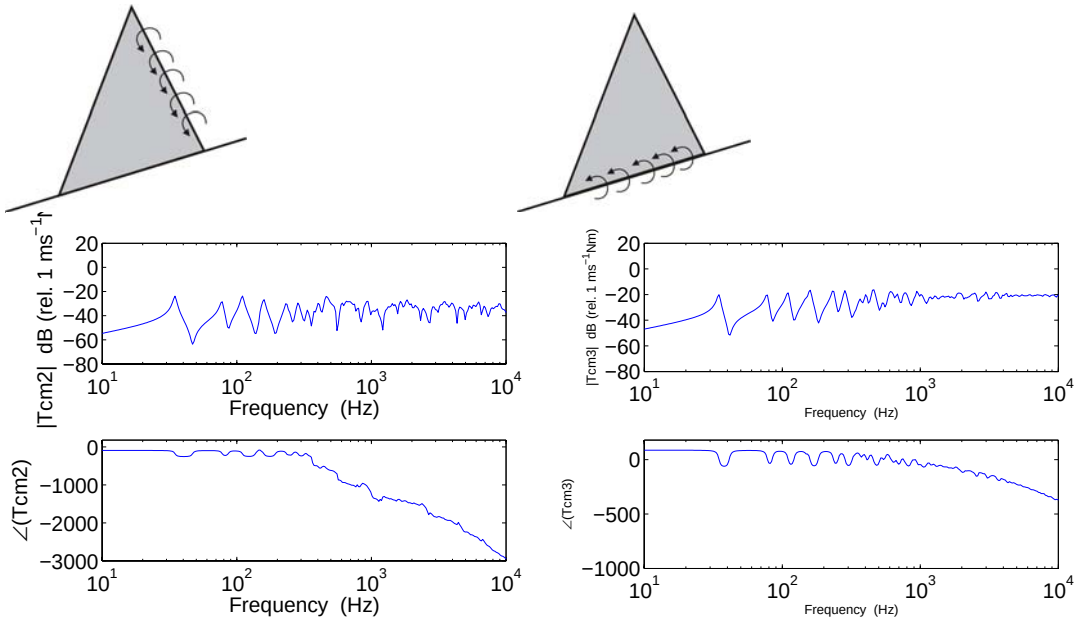

e. Bending moment on the right edge of the actuator

f. Bending moment on the base of the actuator

Figure 29: *Bode diagrams of the open loop transfer function for a resiliently supported panel controlled by a triangular piezoelectric actuator for an infinite stiffness in translation for each effect of the triangular piezoelectric.*

The previous analysis clearly shows that the non collocation between the sensor and the actuators actions is responsible for instability since it causes phase lags that bring the sensor-actuator open loop to the conditional stability domain.

The first drop in the amplitude of the global response is mainly due to the moment produced on the base edge. The drops that can be observed at higher frequencies are due to the combination of all moments and forces.

Figure 30 presents the laboratory set up for the measurements of open loop functions and implementation of the feedback control loops on the panel. The aluminium panel on which are bonded the 16 piezoelectric actuators is mounted on a Plexiglas box in which a white sound is produced by a loudspeaker. The sensors are accelerometers placed at the top of the triangular actuator.

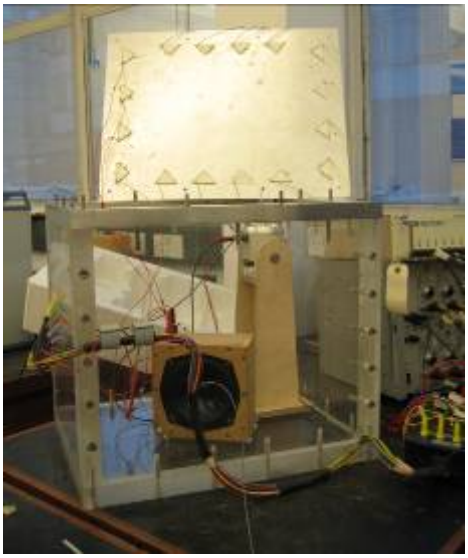

Figure 30: *experimental test rig with smart panel*

Figure 31 presents the measured open loop response between the sensor and the actuator which is very close to the Figure 26 since mounting of the panel is similar to a clamped mounting. A good modelisation of the system is therefore a resiliently supported panel mounted with very stiff springs in rotation and translation.

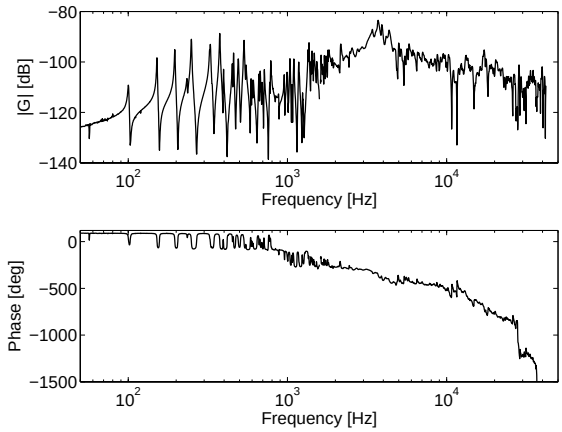

Figure 31: *Measured open loop response of the panel*

4.3. Performance

The performance study is based again on the observation of the velocity of the control point and the kinetic energy of the panel. The control point is taken this time at the top of the first actuator next to the corner in $(x_1, y_1) = (56,40)mm$ (black actuator on Figure 21). Only the effect of one actuator is taken in account.

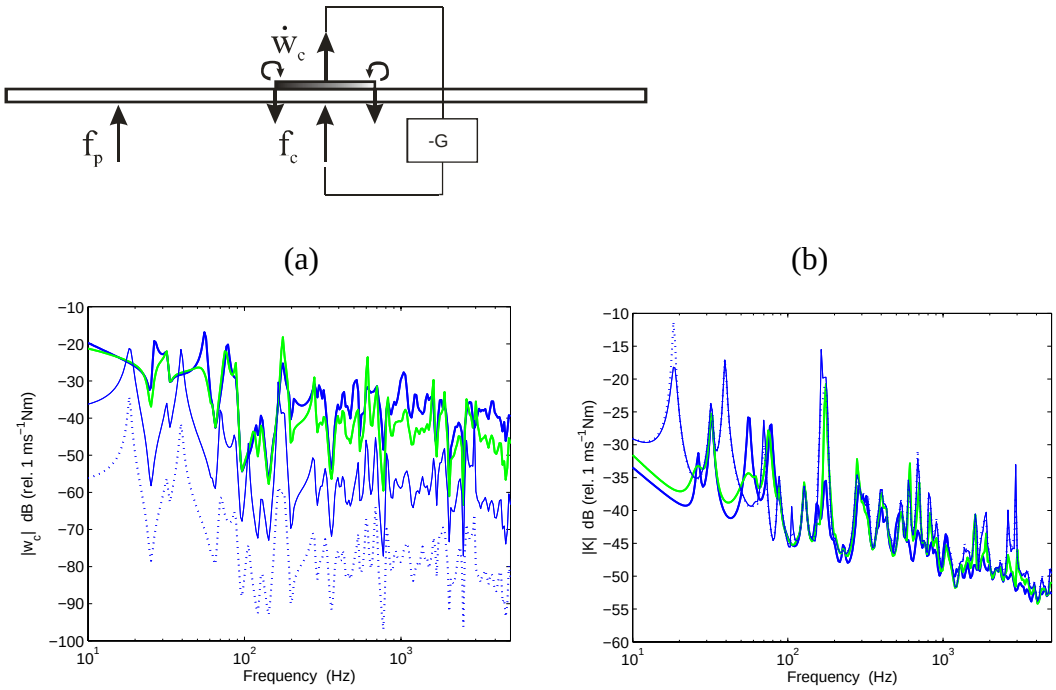

Figure 32: *Amplitude of the response to the control point (a) and kinetic energy of the panel (b) for a free panel controlled by a triangular piezoelectric actuator and some values of gain:* $g = 0,\ g = 1,\ g = 10,\ g = 10^6$ *(respectively thick black, grey, thin black, dotted)*

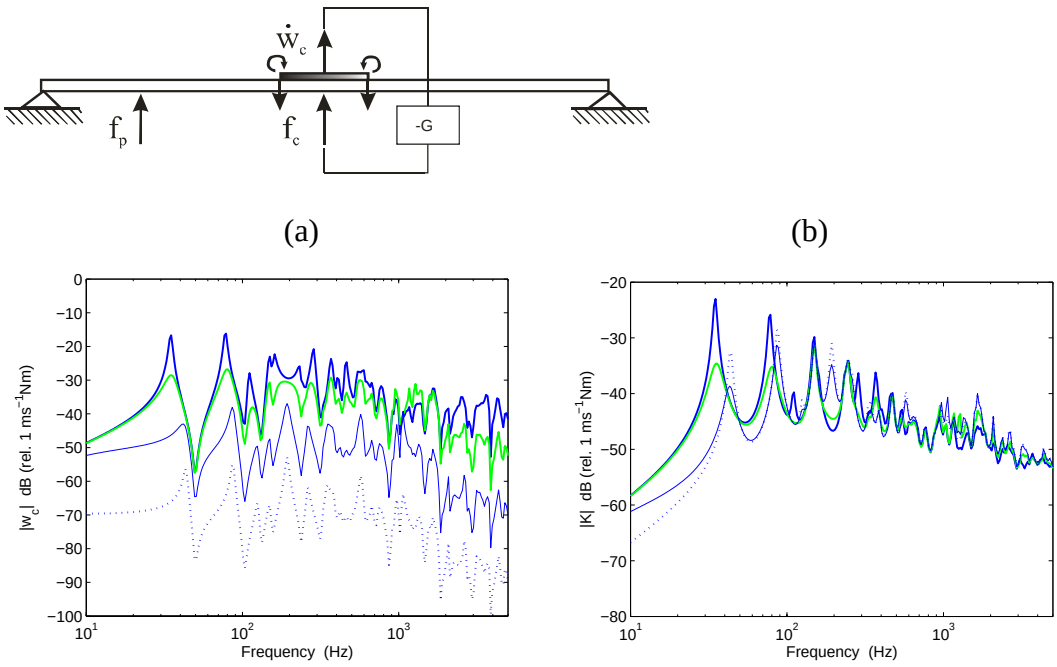

Figure 33: *Amplitude of the response to the control point (a) and kinetic energy of the panel (b) for a resiliently supported panel with an infinite stiffness in translation controlled by a triangular piezoelectric actuator and some values of gain:* $g = 0,\ g = 1,\ g = 10,\ g = 10^6$ *(respectively thick black, grey, thin black, dotted)*

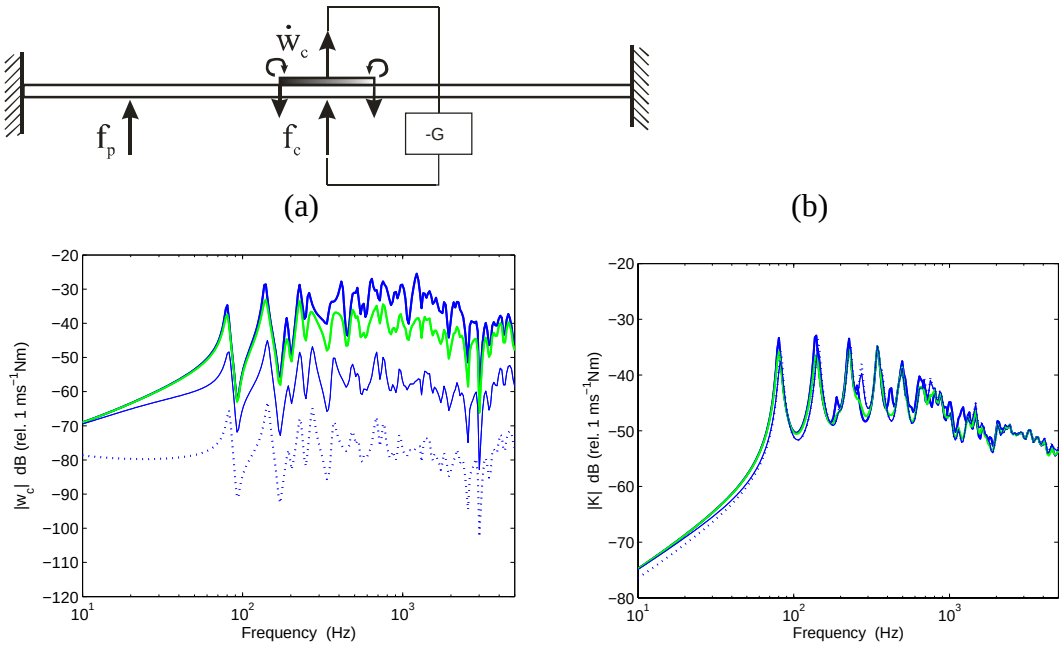

Figure 34: *Amplitude of the response to the control point (a) and kinetic energy of the panel (b) for a resiliently supported panel with an infinite stiffness in translation and in rotation controlled by a triangular piezoelectric actuator and some values of gain:* $g = 0,\ g = 1,\ g = 10,\ g = 10^6$ *(respectively thick black, grey, thin black, dotted)*

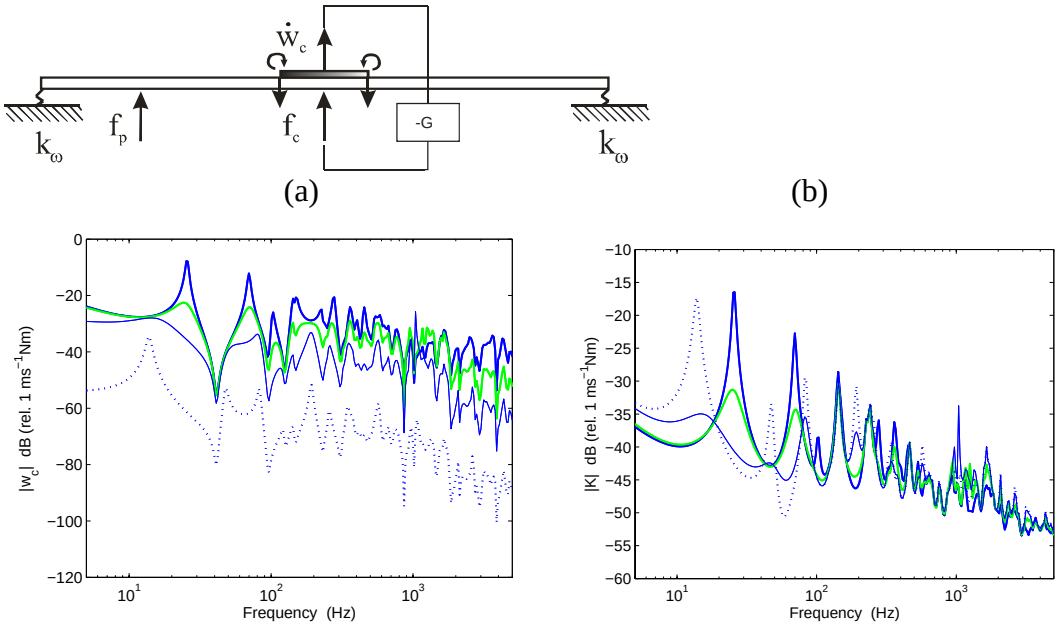

Figure 35: *Amplitude of the response to the control point (a) and kinetic energy of the panel (b) for a resiliently supported panel with stiffness of* $k=10^{-2}$ *in translation controlled by a triangular piezoelectric actuator and some values of gain:* $g = 0,\ g = 1,\ g = 10,\ g = 10^6$ *(respectively thick black, grey, thin black, dotted)*

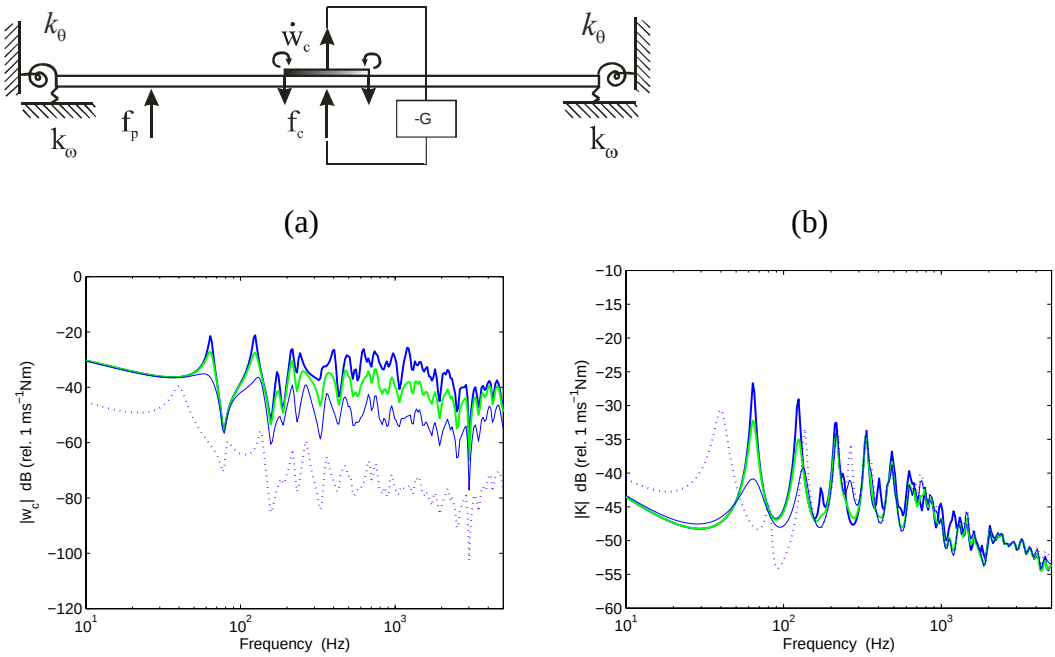

Figure 36: *Amplitude of the response to the control point (a) and kinetic energy of the panel (b) for a resiliently supported panel with stiffness of* $k=10^{-2}$ *in translation and in rotation controlled by a triangular piezoelectric actuator and some values of gain:* $g=0$, $g=1$, $g=10$, $g=10^6$ *(respectively thick black, grey, thin black, dotted)*

We can see on Figures 32 to 36 that the performances are very close to the ones of the single force control. Also the system produces the same pinning effect observed for the control system with the point force actuator. A notable difference in Figure 34 comes from the fact the control point is this time closer to the edge than for the study of the chapter 2. Thus the gain will have to be chosen in consequence once more in order to offer the best performances and stability.

In summary, we can note on the plots of the velocity of the control point in Figures 32a,b to 36a,b the same characteristics found in the previous chapter, that is:

1) the peaks are more lightened for higher gain until the properties of the system are modified
2) this phenomenon is more pronounced in the lower frequencies where we expect the control system to be efficient.
3) the damping is the most efficient in the case of the clamped panel .

5. PARAMETRICAL STUDY

The aim of velocity feedback is to generate active damping, which is particularly effective at resonance frequencies where in fact the response of the structure is principally controlled by damping. For a given resonance frequency, the maximum reduction of vibration R_{20} that can be generated by the control loop is given by ratio between the velocity at the error sensor without control and with the maximum control gain $H_{max.}$ The ratio is given by:

$$R_{20} = \frac{\left|\dot{w}(\omega_k)_{\max\,\text{control}}\right|}{\left|\dot{w}(\omega_k)_{\text{no control}}\right|} = \frac{1}{\left|1 + H_{\max} Y_{cc}(\omega_k)\right|} \ . \tag{34}$$

When the locus of the open loop sensor–actuator FRF crosses the real negative axis at frequency ω_0, the maximum control gain H_{max} that guarantees stability is given by the following formula.

$$H_{\max} = 1/\delta_0 = 1/\left|G_{cc}(\omega_0)\right| = -1/\text{Re}\{G_{cc}(\omega_0)\} \ . \tag{35}$$

For low frequency resonances such that the locus-circles starts from the origin and are aligned along the real positive axis, the value $G_{cc}(\omega_k)$ can be approximated by the amplitude δ_2 as presented on Figure 37 where the *k*-th resonance circle crosses the real axis [25]. Therefore, Equation (34) can be simplified into the following formula.

$$R_{20} \cong \frac{\delta_o}{\delta_o + \delta_2} = 1 + \delta_{0k} \tag{36}$$

where δ_{ok} denotes the ratio between the amplitude of *k*-th "resonant circle" δ_2 and the inverse of the maximum control gain δ_0 in the Nyquist plot of the open loop of the sensor–actuator FRF. This equation gives the approximate maximum reduction R_{20} of the error sensor velocity at the *k*-th resonance frequency. This formulation provides a simple approach for the derivation of the control effectiveness at low frequency resonances based on the predicted or measured open loop sensor–actuator frequency response function.

The performance of the system at low frequencies is related to high amplitude of the response in this frequency range, e.g. to big loops on the right hand side of the Nyquist plot. At the opposite, stability is given by relatively small loops on the left hand side of the Nyquist plot. As a consequence the criterion using the ratio between these two values is able to assess both performance and stability: a high ratio means, good performance and stability, and a low ratio means bad ones.

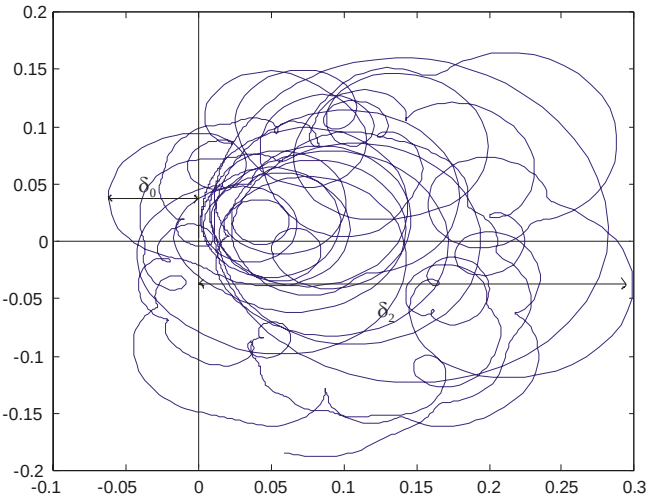

Figure 37: *Values of the parameters δ_0 and δ_2 on the Nyquist plot used to calculate the ratio R_{20}*

5.1. Influence of the transversal spring

In this section the rotational stiffness are taken to be zero. The transversal stiffness increase from 10^{-4} to10^{-3}.

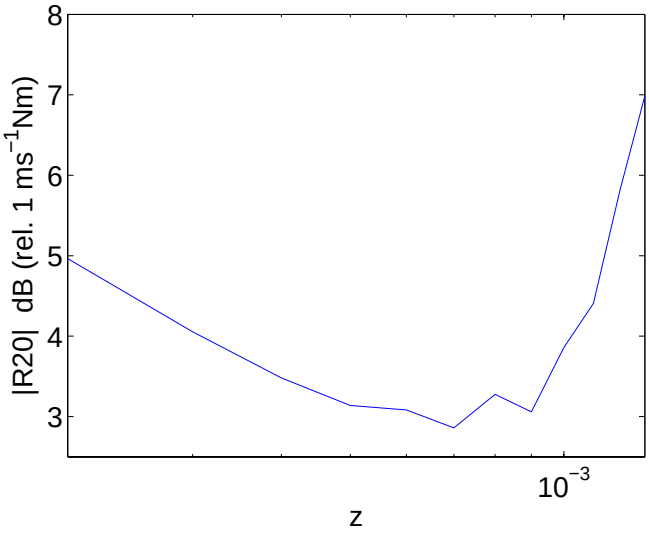

Figure 38: *Evolution of the ratio function of the stiffness of the springs in translation for a stiffness in rotation equal to zero.*

Figure 38 presents the plot of the ratio $R_{20} = 10\log 10\left(1+\frac{\delta_2}{\delta_0}\right)$. The first part of the curve has a slope slightly negative which is probably due to errors in the approximation of δ_2 of the sampling of the simulated sensor-actuator response function. Starting at 10^{-3} approximately the slope is very high; the system becomes more and more stable as the mounting axial stiffness is increased. It confirms the

results of the chapter 3. A very stiff panel therefore will be more stable and will allow us to implement higher control gains.

5.2. Influence of the rotational spring

In this section the transversal stiffness are taken to be infinite. The rotational stiffness increase from 10^{-4} to10^{-3}.

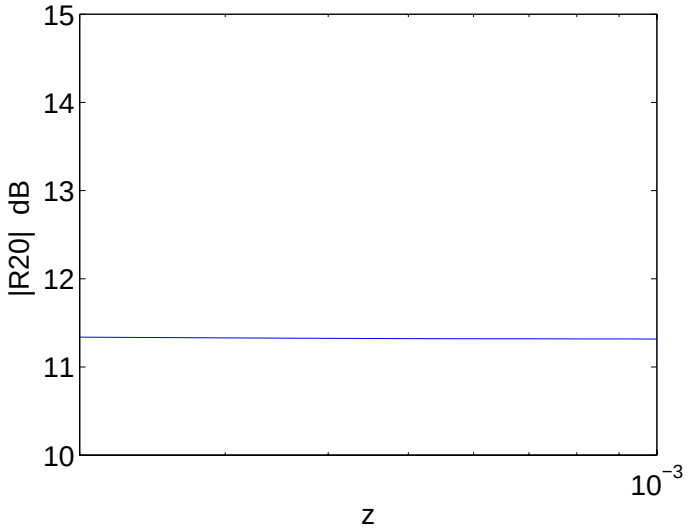

Figure 39: *Evolution of the ratio function of the stiffness of the springs in rotation for an infinite stiffness in translation.*

The effect of the rotational springs on the stability is negligible compared to the one of the transversal spring. Thus the main lever on which we will have to act to improve stability is the translation stiffness since a low rotational stiffness will not be handicap for stability.

6. CONCLUSION

In this work it has been shown that the triangular piezoelectric actuators can give very good results in direct velocity feedback control of a resiliently mounted panel.

The boundary conditions and therefore the mounting of the panel to the frame have a big influence on the performance and the stability of the control system. The rotational and translation effect on the edge have been studied. The translation stiffness appears to be the most important for the performances as for the stability but the rotational stiffness also have a slight influence. A high stiffness in translation and rotation will increase considerably the system's stability and allow an implementation of much higher gain value for the feedback control loop.

This study also points the fact that, even if the system remains stable for very high gain values, a too high gain might change the system itself by pining the panel at the control point. In this case the control is not efficient anymore, the system presents new resonance's frequencies and new picks. The optimum gain is to be found by a compromise between best performance and stability.

In any case the stability will be better for very high stiffness. Then, this kind of active system can be very interesting since the feedback loop is very simple to implement, the complications come from the weight and size of the filters and amplifiers which are used for the actuators since each one is driven independently.

Other parameters have an effect on the performance and the stability of the system like the parameters of the actuator such as its weight or its dimensions also the mass of the accelerometer can change the comportment of the system. The robustness of the control system is also to be studied since lots of parameters might vary in practice, so that the system remains efficient when it happens.

Although the control system could be improve, active control using triangular shaped piezoelectric actuators can bring a significant advance in transport since the analyse of its performance and stability gives great results and that the system on itself is small and light. These properties constitute huge advantages in the industry of transport rather automobile or aeronautics.

7. FUTURE WORK

As explained in the Chapter 4 triangular shaped piezoelectric actuators can still generates instabilities and increase vibrations on the panel instead of reducing them for some frequencies. As this effect is connected to the boundary conditions that are the mounting of the panel to the frame, a practical study of what mounting should be employed to have the best performances should be carried out, as well as a study of the materials to use for this mounting in order to have the best performances and stability. The mounting can significantly help to stabilise the system so that high gain could be implemented.

Other tools can be used to stabilise the system, to be even more efficient or in case the mounting is imposed by the application. Since no spillover effects occur below 5 kHz, a low pass filter can be used with cut off frequencies situated below the first frequency where spillover effects occur.

Another way of reducing the spillover effect is to use phase compensators that are able to modify the Nyquist plot in such way that all loops are situated in the right hand side of the Nyquist plot. In that case, very high gains can be used without reaching instability.

However using such devices make system control much more complicated to use and generally heavier which is very bad since one of the purpose of the system is to reduce weight. Researches still need to be made for these systems to be interesting in our case.

Another issue is the power supply of the piezoelectric actuator which usually needs high voltages to be efficient. This is generally a problem for embarked systems.

ACKNOWLEDGEMENTS

I would like to thank Professor Paolo Gardonio who supervised my work at the ISVR. I am very thankful to the patience he had with me, for the help and the trust he gave me.

I am also grateful to the acoustic department at Renault and particularly to Sebastien Chaigne, who supported this project and gave me the opportunity to do a very interesting work.

I would also like to address my thanks to all the ISVR staff, which has always helped me. In particular Yohko Aoki spent much time helping me to get started with the project. I would like to thanks Professor Stephen J. Elliott for welcoming me in his team and Mrs Joyce Shotter for helping me when I needed.

References

1. D.J.Thompson and J.Dixon. 2004. vehicle noise, in chapter 6 of advanced applications in acoustic noise and vibration, edited by F.J.Fahy, J. Walker, Spon press.
2. F.J.Fahy. 1998. Fundamentals of Noise and Vibration Control, in chapter 5 of Fundamentals of Noise and Vibration edited by F.J. Fahy and J. Walker, E & FN Spon.
3. P.A.Nelson and S.J.Elliott. 1992. Active Control of Sound. New York, Academic Press.
4. S.J.Elliott. 2001. Signal Processing for Active Control. London, Academic Press.
5. A.Preumont. 2002. Vibration Control of Active Structures. London, Kluwer Academic.
6. R.L.Clark, W.R.Saunders and G.P.Gibbs. 1998. Adaptive Structures. 1st Edition. New York, John Wiley & Sons, Inc.
7. B.Petitjean and I.Legrain. Feedback controllers for active vibration suppression. Journal of Structural Control, **3**[1-2], 111-127. 1996.
8. P.Gardonio, E. Bianchi and S.J.Elliott. Smart panel with multiple decentralised units for the control of sound transmission. Part I: Theoretical predictions. Part II: Design of the decentralised control units. Part III: Control system implementation. Journal of Sound and Vibration, No. 274, 163-232. 2004.
9. Elliott, S.J., Gardonio, P., Sors, Thomas C., and Brennan, M.J. Active vibroacoustic control with multiple local feedback loops. Journal of the Acoustical Society of America, 111[2], 908-915. 2002.
10. J.Q.Sun. Some observations on physical duality and collocation of structural control sensors and actuators. Journal of Sound and Vibration, 194, 765-770. 1996.
11. Jayachandran, V., Sun, J.Q. Unconditional stability domains of structural control systems using dual actuator-sensor pairs. Journal of Sound and Vibration, 208[1], 159-166. 1997. Academic Press.
12. M.J.Balas. Direct velocity control of large space structures. Journal of Guidance and Control, 2, 252-253. 1979.
13. Gardonio, P and Elliott, S.J. Modal response of a beam with a sensor-actuator pair for the implementation of velocity feedback control. Journal of Sound and Vibration, 284[1-2], 1-22. 2005.
14. Johnson, M.E. and Elliott, S.J. Active control of sound radiation using volume velocity cancellation. Journal of the Acoustical Society of America, **98**[4], 2174-2186. 1995.
15. Gardonio, P., Lee, Y.S., Elliott, S.J., and Debost, S. Analysis and measurement of a matched volume velocity sensor and uniform force actuator for active structural acoustic control. Journal of the Acoustical Society of America, **110**[6], 3025-3031. 2001.

16. S.J.Elliott, P.Gardonio, T.C.Sors and M.J.Brennan. Active vibro-acoustic control with multiple feedback loops. Journal of the Acoustical Society of America, **111**(2, 908-915. 2001.

17. P.Bianchi and S.J.Elliott. Smart panel with multiple decentralised unit for the control of sound transmission. Part 1 Theoretical prediction. Part 2: Design of the decentralised control units. Part 3: Control system implementation. Journal of the Acoustical Society of America, **274**,163-232. 2004.

18. P.Gardonio and S.J.Elliot. Smart panels with velocity feedback control systems using triangularly shaped strain actuators. Journal of the Acoustical Society of America, **117**(4), 2046-2064. 2005.

19. D.Emo, P.Gardonio. Decentralised velocity feedback control unit using triangular piezoelectric actuator. ISVR Technical Memorandum Nº 950. 2005.

20. Y.Aoki, P.Gardonio, D.Emo and S.J.Elliott. Stability and controllability of velocity feedback loops with triangularly shaped Piezoelectric actuators. Active 2006, the 2006 International Symposium on Active Control of Sound and Vibration, Adelaide, Australia, 18-20 September 2006.

21. C.Hong, P.Gardonio and S.J.Elliott. Active control of resiliently mounted beams using triangular actuator. Accepted for publication in the Journal of Sound and Vibration. Academic Press-Elsevier, London. 2006.

22. P.Gardonio and M.J.Brennan. 2004, Mobility and impedance methods in structural dynamics, chapter 9 in advanced applications in acoustics, noise and vibration", edited by F.J. Fahy and J. Walker. Spon Press.

23. A. Preumont. 2002. Vibration control of active structures. Kluwer Academic.

24. L.Meirovitch. 1990. Dynamics and Control of Structures. New York, John Wiley & Sons.

25. Yohko Aoki, P. Gardonio and S.J. Elliott. *Parametric Study of a Piezoelectric Patch-Accelerometer Pair for Velocity Feedback Control.* Institute of Acoustics Spring Conference 2006, ISVR, University of Southampton, UK, 3-4 April 2006.